Evolution of Bishop Tuff Rhyolitic Magma Based on Melt and Magnetite Inclusions and Zoned Phenocrysts

ALFRED T. ANDERSON[1]*, ANDREW M. DAVIS[2] AND FANGQIONG LU[1]†

[1]DEPARTMENT OF THE GEOPHYSICAL SCIENCES, THE UNIVERSITY OF CHICAGO, 5734 S. ELLIS AVE., CHICAGO, IL 60637, USA

[2]ENRICO FERMI INSTITUTE, THE UNIVERSITY OF CHICAGO, CHICAGO, IL 60637, USA

The evolution of large bodies of silicic magma is an important aspect of planetary differentiation. Melt and mineral inclusions in phenocrysts and zoned phenocrysts can help reveal the processes of differentiation such as magma mixing and crystal settling, because they record a history of changing environmental conditions. Similar major element compositions and unusually low concentrations of compatible elements (e.g. 0·45–4·6 ppm Ba) in early-erupted melt inclusions, matrix glasses and bulk pumice from the Bishop Tuff, California, USA, suggest eutectoid fractional crystallization. On the other hand, late-erupted sanidine phenocrysts have rims rich in Ba, and late-erupted quartz phenocrysts have CO_2-rich melt inclusions closest to crystal rims. Both features are the reverse of in situ crystallization differentiation, and they might be explained by magma mixing or crystal sinking. Log(Ba/Rb) correlates linearly with log(Sr/Rb) in melt inclusions, and this is inconsistent with magma mixing. Melt inclusion gas-saturation pressure increases with CO_2 from phenocryst core to rim and suggests crystal sinking. Some inclusions of magnetite in late-erupted quartz are similar to early-erupted magnetite phenocrysts, and this too is consistent with crystal sinking. We argue that some large phenocrysts of late-erupted quartz and sanidine continued to crystallize as they sank several kilometers through progressively less differentiated melts. Probable diffusive modification of Sr in sanidine phenocrysts and the duration of crystal sinking are consistent with an evolutionary interval of some 100 ky or more. Crystal sinking enhanced the degree of differentiation of the early-erupted magma and points to the importance of H_2O (to diminish viscosity and enhance the rate of crystal sinking) in the evolution of silicic magmas.

KEY WORDS: *crystal settling; differentiation; melt inclusions; rhyolite; trace elements*

BACKGROUND, SAMPLE SELECTION AND METHODS

Compared with other large-volume, silicic ash-flow tuffs [see reviews by Smith & Bailey (1966), Smith (1979) and Hildreth (1981)], the 0·76-My-old Bishop Tuff is relatively uniform in major element composition, mostly ranging from 75·5 to 77·6 wt % SiO_2. However, it has conspicuous trace element variations and shares with other silicic ash-flow tuffs increases in both phenocryst content and Fe–Ti oxide temperature with eruptive sequence (Hildreth, 1977, 1979). The Bishop Tuff was first documented by Gilbert (1938), and its stratigraphic relations and petrology have been studied by Sheridan (1965), Hildreth (1977, 1979), and Wilson & Hildreth (1997). Despite the many studies of the Bishop Tuff, the origins of both its high-silica magma and particularly of its compositional zonation have remained controversial (Hildreth, 1977, 1979, 1981; Michael, 1983; Cameron, 1984; Lu, 1991; Dunbar & Hervig, 1992; Hervig & Dunbar, 1992; Lu *et al.*, 1992*a*). Our studies aim to elucidate the processes of differentiation of the Bishop magma by documenting the evolutionary changes recorded in zoned crystals and inclusions of melt and crystals within phenocrysts.

The trace element work reported here is based on the study by Lu (1991) and is closely related to that of Wallace *et al.* (1999). The latter paper focuses on volatiles. The data comprise two sets: (1) the Lu–Skirius suite of melt inclusions and phenocrysts, which were collected in 1987 and analyzed between 1987 and 1992 (Skirius, 1990;

*Corresponding author. Telephone: +1-773-702-8138. Fax: +1-773-702-9505. e-mail: <canderso@midway.uchicago.edu>

†Present address: 11304 Cedarcliff Dr., Austin, TX 787530, USA.

Lu, 1991) and (2) the Wallace suite of melt inclusions, most of which were sampled and studied between 1991 and 1995 and were based on the emerging stratigraphic framework of Wilson & Hildreth (1997). Many inclusions in both datasets were analyzed for both volatile and non-volatile elements, although some inclusions were analyzed only for H_2O and CO_2 or only for non-volatile elements. Both sets of samples have now been referenced to the stratigraphic framework of Wilson & Hildreth (1997).

The new, detailed stratigraphy of the Bishop Tuff (Wilson & Hildreth, 1997), together with other work, emphasizes three important conceptual differences from Hildreth's earlier work (1979): (1) plinian fall deposits were erupted synchronously with most, and possibly all of the ash-flow deposits; (2) different types of pumice clasts were codeposited (E. W. Hildreth, personal communication, 1996); (3) separate segments of the ring-fault system were active as vents for various durations and in part concurrently, as first noted by Hildreth & Mahood (1986).

Sample locations for the pumice clasts used in this study are indicated in Fig. 1. Their stratigraphic relations are detailed in the Appendix and summarized below. [See also fig. 2 of Wallace *et al.* (1999).]

We use a simplified quasichronological nomenclature and refer to early-, mid- and late-erupted parts of the Bishop Tuff. The ignimbrite units of Wilson & Hildreth (1997) can be identified with ash-flow lobes of Hildreth (1977) and with our early, mid- and late-designations as follows: Ig1E, Gorges and Chidago lobes (early); Ig2E, Tableland lobe (mid); Ig2N, Adobe lobe (late); Ig2NW, Mono lobe (late). All plinian fall strata studied in this work are 'early': they lack pyroxene-phyric pumice and Glass Mountain rhyolite lithic clasts. Wilson & Hildreth (1997) used the occurrence of Glass Mountain rhyolite lithic clasts and the occurrence of pyroxene-phyric pumice as stratigraphic marker horizons, and interpreted them to reflect the opening of new vents, which began to tap a different portion of the magma as well as wall rock. Ig2E (Tableland lobe) is partly synchronous with fall unit F9 and contains a wide range of pumice compositions that form a transition to northern ignimbrite units (Ig2N), which are also interpreted to be partly synchronous with Ig2E.

The Bishop Tuff samples studied in this work include both pumice fall and ignimbrite deposits. Our pumice fall samples represent the following units in Wilson & Hildreth's (1997) stratigraphy: F5 (BT87-2), F6 (BT87-3), F5 and/or F6 (BT87-20 to -23) and F7 (BT87-5 to -9). Our ignimbrite samples are of Ig1Eb (BT87-10 to -16, -24 and -25), which is synchronous with parts of F6, F7 and F8; of Ig2E (BT87-131 to -133, and LV81-2 to -7), which is partly synchronous with F9; of Ig2Na (BT87-103 to -123) and Ig2NWa (our sample locality 6, samples 327), both of which are partly contemporaneous with

Ig2E; and of Ig2NWb (BT87-32 to -45, LV81-17 and -18). The age sequence is from F5 (earliest) to Ig2NWb (latest), but includes partially synchronous units. Melt inclusions suitable for study occur in only a subset of the above samples, but we mention other samples from which we studied sanidine, plagioclase and magnetite crystals. The Appendix and Table 1 list only those samples that have electron and/or ion microprobe analyses of glass inclusions. The mineral analyses are presented in some of our graphs and were tabulated by Lu (1991).

We studied pumice clasts individually to minimize possible coeruptive magma mixing whereby codeposited and even coerupted clasts might derive from a range of depths (Blake & Ivey, 1986; Spera *et al.*, 1986) and/or different vents. Magma that forms a single clast of pumice is likely to be least affected by eruptive mixing (Schuraytz *et al.*, 1989).

Our findings are, in part, inconsistent with *in situ*, gas-saturated crystallization: (1) some sanidine phenocrysts are reversely zoned (Ba-rich rims); (2) some magnetite included in some late-erupted quartz phenocrysts is compositionally similar to Hildreth's (1977) low-T magnetite (early-erupted); (3) some late-erupted quartz phenocrysts contain multiple melt inclusions, the more differentiated (CO_2-poor) of which preferentially occur in the cores of the quartz phenocrysts and have relatively low gas-saturation pressures. We argue that these features are best explained by crystal sinking.

TEXTURES AND MINERALOGY OF PUMICE CLASTS

Gilbert (1938), Sheridan (1965) and Hildreth (1977, 1979) reported compositions and/or textures of Bishop ash-flow tuffs, pumice clasts and phenocrysts. Below is a brief summary taken mostly from Hildreth (1979) and our observations. In the early- and mid-erupted Bishop Tuff, phenocrysts of quartz, sanidine and plagioclase occur in proportions of about 3:3:1. The proportions are about 2:3:1 in the late-erupted Bishop Tuff. Biotite and magnetite comprise up to ~4 vol. % of Bishop phenocrysts. Pyroxenes are absent in the early-, but are up to ~1 vol. % of the total crystals in some mid- and late-erupted pumice clasts of the Bishop Tuff. Phenocryst content varies widely; Hildreth (1979, p. 49) gave 5–25 vol. % (void free). Pumices with >15% phenocrysts are more abundant in late-erupted units, but also occur in early units.

The sizes of phenocrysts of quartz and sanidine range from ~0·3 mm to ~3 mm in maximum dimension in early- and mid-erupted pumice. Late-erupted phenocrysts of quartz and sanidine range to ~5 mm. Polycrystalline aggregates of quartz and feldspar are rare. Multiple crystal fragments line many large vesicles in late Bishop
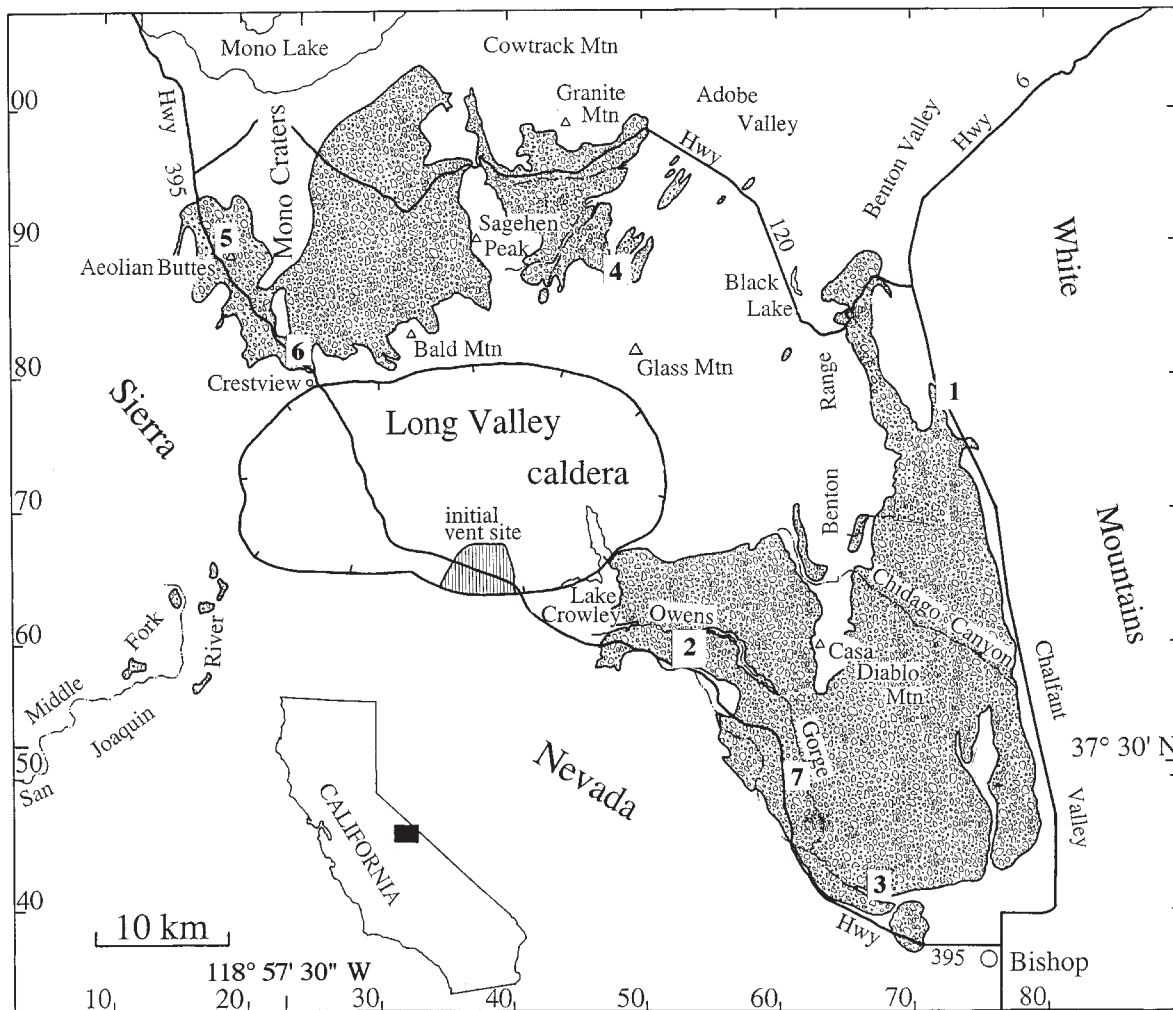
Fig. 1. Map of the Bishop Tuff and Long Valley caldera (after Wilson & Hildreth, 1997). The early-erupted Bishop Tuff includes pyroxene-free plinian pumice-fall and ash-flow deposits located mostly south and east of Long Valley caldera. The late-erupted Bishop Tuff consists of pyroxene-phyric ash-flow deposits located mostly to the north of the caldera, but includes some pumice and ash deposited in the south-east sector. Wilson & Hildreth (1997) showed that the Bishop deposits north of the caldera erupted from a northern vent system whereas the southeastern deposits erupted from southern and eastern vent systems. Products of the separate vent systems were partly synchronous and some predepositional mixing probably occurred. Our samples are from early- and mid-erupted units south and east of the caldera (locations 1, 2, 3 and 7) and later erupted units from north of the caldera (locations 4, 5 and 6). Detailed locations and descriptions of samples are given in the Appendix. (See text for definitions of early, mid and late as used in this work.) Universal Transverse Mercator grid marks run from 4140 to 4200 km along the side and from 310 to 380 km (the 41 and 3 are omitted).

pumice, but such fragments are fractured and all crystal fragments in a single vesicle are of the same mineral except for small crystals of dark minerals that plausibly were included in the host quartz or feldspar. It is likely that the fragments are pieces of single large crystals that shattered as melt inclusions ruptured (Best & Christiansen, 1997) and vesiculated. Almost all quartz and feldspar phenocrysts are solitary crystals.

The isolation of solitary phenocrysts suggests nucleation and growth in a melt-rich magma rather than derivation from crystal-rich margins of a magma body. Solitary nucleation and growth is consistent with supercooling

caused by gas-saturated decompression, rather than by marginal cooling and crystallization attached to the margins of the magma body.

The late-erupted Bishop Tuff contains trace amounts of dark (gray to black) and streaked (white and dark) pumice clasts (Hildreth, 1985). Most dark pumice is virtually aphyric. White streaks commonly have phenocrysts, most of which are fractured and contain burst melt inclusions. E. W. Hildreth (personal communication, 1990) noted that dark pumice is also present, but much less abundant, in the early-erupted Bishop Tuff. The SiO_2 content of most dark pumice is ~ 73 wt %, but

Table 1: Chemical compositions of selected Bishop Tuff melt inclusions in quartz

Clast:*	5D-Lu	8B	11B	11B	6A	6A	17A	17A	17A	32W	327-3	327-3	Av.
Xtal–incl.:†	Lu1-1	H4	Lu-1	Lu-2	B7-1	B7-2	6-1	6-2	7-1	1	1-2-2	1-2-3	error**
Location:‡	1	1	1	1	1	1	5	5	5	5	6	6	
Stratig.§	F7	F7	Ig1Eb	Ig1Eb	F7	F7	Ig2NWb	Ig2NWb	Ig2NWb	Ig2NWb	Ig2NWa	Ig2NWa	
Size:¶	220	145	185	150	180	150	170	90	170	110	350	90	
Devitr.:	none	none	slight	slight	none	none	slight	slight	slight	complete	none	none	
SiO₂	77·6	77·4	77·6	77·6	77·6	78·1	77·6	77·5	77·1	78·3	77·7	78·6	0·7
Al₂O₃	12·3	12·7	12·6	12·5	12·6	12·4	12·2	12·4	11·9	11·6	12·1	11·8	0·4
Na₂O	4·49	4·17	3·78	3·74	4·15	3·60	3·54	3·84	4·38	4·08	3·36	3·02	0·49
K₂O	4·69	4·80	5·24	5·07	4·67	4·87	5·50	5·11	5·59	5·15	5·45	5·33	0·24
CaO	0·41	0·43	0·45	0·43	0·44	0·42	0·47	0·44	0·44	0·42	0·50	0·43	0·01
FeO	0·65	0·66	0·66	0·66	0·67	0·66	0·69	0·69	0·58	0·61	0·71	0·63	0·03
MgO	0·02	0·03	0·03	0·03	0·02	0·02	0·03	0·04	0·03	0·03	0·05	0·04	0·01
Total	95·8	93·9	96·0	96·1	94·9	95·5	93·3	95·6	96·5	96·4	95·5	96·0	
H₂O	5·54	5·76	5·53	5·68	5·22	5·11	4·05	4·14	3·82	3·50	3·18	3·77	
CO₂	19	35	321	135	46	45	536	531	221	71	962	405	
P_{sat}††	1701	1859	2134	1958	1561	1495	1844	1882	1247	leaked	2053	1507	
Li	85·4	86·3	60·4	56·0	84·4	84·0	15·2	27·4	24·7		52·0	49·4	1·3
Be	6·76	6·34	5·71	6·45	6·70	6·31	1·92	3·05	2·77	4·89	3·29	3·75	0·24
B	70·4	67·5	61·7	61·8	63·9	64·7	35·2	43·9	46·3	48·2	49·6	50·5	1·2
F	398	556	366	276	361	399	139	223	187	165	134	202	34
Mg	162	150	175	182	182	181	244	233	198	209	369	272	2·1
Ca	3041	2718	3134	3187	3270	3175	3115	2941	2908	3012	3460	3005	9
Sc	3·07	4·04	2·82	1·81	2·30	4·75	3·59	2·69	2·96	2·08	3·46	3·47	1·05
Ti	449	423	508	499	470	488	565	518	538	505	557	511	5
V	4·70	3·61	3·10	4·65	3·57	3·68	3·86	2·53	2·63	4·74	1·91	2·47	0·59
Mn	143	137	123	136	132	129	121	101	122	102	99·7	109	26
Fe	4051	3510	3470	4092	3483	3666	4431	3595	3907	3488	4963	4224	685
Rb	183	191	158	181	170	163	165	163	177	140	103	146	3
Sr	1·93	1·72	1·27	1·25	1·41	0·95	4·14	3·82	1·81	2·13	19·4	2·31	0·24
Y	25·2	22·0	23·2	21·8	21·7	22·0	19·2	20·0	22·4	18·7	18·4	19·1	0·6
Zr	86·2	83·2	97·8	85·1	85·3	87·5	93·6	99·4	91·8	75·7	88·1	84·2	2·0
Nb	29·7	30·8	32·2	27·7	26·0	26·3	25·1	25·5	29·0	25·3	24·2	24·3	1·0
Cs	6·21	5·94	4·83	5·95	5·18	4·52	4·94	4·23	4·70	4·05	3·14	4·74	0·67
Ba	1·36	1·82	1·85	1·45	1·51	1·05	9·22	8·59	3·14	3·45	107	4·79	0·62
La	15·0	13·4	18·4	17·9	16·9	16·5	26·1	26·3	21·9	19·1	25·9	20·8	0·3
Ce	36·8	33·7	42·0	42·8	40·2	38·1	55·2	58·1	49·9	42·8	55·0	46·0	0·7
Pr	3·93	3·86	4·64	4·80	4·21	3·99	5·65	6·17	5·48	5·06	5·60	4·31	0·30
Nd	12·3	12·8	14·6	14·3	13·0	12·3	16·8	15·9	17·0	13·2	16·1	14·6	0·9
Sm	2·66	2·45	2·63	2·38	2·23	2·50	3·14	3·11	3·32	2·69	3·42	3·03	0·20
Eu	0·019	<0·031	0·027	<0·030	0·024	0·025	0·145	0·113	0·066	0·017	0·306	0·022	0·030
Gd	3·89	2·96	3·19	3·10	3·53	3·06	3·20	2·99	4·11	2·49	3·05	3·12	0·51
Tb	0·669	0·575	0·611	0·414	0·483	0·519	0·518	0·508	0·633	0·645	0·638	0·329	0·096
Dy	3·93	3·32	3·31	3·26	3·13	3·30	2·99	3·34	4·02	2·45	3·06	3·34	0·30
Ho	0·710	0·706	0·728	0·758	0·662	0·598	0·679	0·763	0·819	0·544	0·613	0·676	0·109
Er	2·60	2·55	2·47	2·42	2·45	2·40	2·27	2·13	2·56	1·79	2·37	2·08	0·20
Tm	0·430	0·397	0·406	0·352	0·321	0·283	0·374	0·334	0·385	0·235	0·280	0·365	0·048
Yb	2·32	2·08	2·23	2·43	1·92	1·60	2·22	1·93	2·40	1·80	1·90	1·73	0·24
Lu	0·386	0·353	0·376	0·452	0·304	0·311	0·389	0·344	0·421	0·238	0·307	0·377	0·061
Hf	3·46	3·88	4·74	3·50	3·43	2·85	3·35	3·99	3·94	2·62	3·29	3·13	0·27
Pb	24·2	26·3	29·9	34·8	25·4	23·7	29·7	29·4	33·4	24·4	28·4	31·7	3·4
Th	19·9	22·9	23·0	18·2	17·2	17·1	20·8	20·1	23·9	15·4	17·7	17·9	0·5
U	7·13	9·02	8·08	6·48	6·70	5·97	6·99	7·12	8·48	5·72	5·65	6·26	0·31

Major oxides (electron microprobe, normalized to 100% anhydrous) and H₂O (FTIR) are given in wt %; CO₂ (FTIR) and trace elements (ion microprobe) are in ppm. Totals are observed electron microprobe sums and approximate the difference between 100% and the H₂O content.
*Clast sample number.
†Crystal fragment number–inclusion number.
‡Map location (see Fig. 1 and Appendix).
§Stratigraphic unit of Wilson & Hildreth (1997).
¶Sizes approximate the geometric mean of the largest two diameters in μm.
**Average error is ±1σ based on counting statistics alone.
††P_{sat} is the pressure in bars at which the melt would be saturated with gas (see text).

ranges to significantly lower values (E. W. Hildreth, personal communication, 1990, 1996). Hildreth (1985) reported that the dark and streaked pumice is notably richer in Fe, Sr and Ba than the late-erupted Bishop Tuff. He also reported that the dark color originates from finely dispersed carbon occurring in concentrations up to 0·35 wt % C and having a $\delta^{13}C$ value of about $-25‰$, consistent with a biogenic source.

COMPOSITIONS OF MATRIX GLASSES

Matrix glasses in early and late pumice that we analyzed have practically identical major element compositions: about 77·5 wt % SiO_2, 12·7 wt % Al_2O_3 and 3·5 wt % Na_2O on an anhydrous basis (Lu, 1991). This composition is shared by both melt inclusions (see below) and early-erupted whole pumice clasts (Hildreth, 1979). Concentrations of Na_2O are slightly less in matrix glass than in glass inclusions. Concentrations of K_2O in matrix glasses are similar to those of early-erupted melt inclusions and early-erupted whole rocks, but more variable, ranging from 4·96 to 5·49 wt % for early- and mid-erupted pumice glass, and from 4·76 to 5·52 wt % for late-erupted pumice glass. Possibly leaching and/or weathering have affected the alkalis in some of the matrix glasses.

TEXTURES OF MELT INCLUSIONS

The distribution and features of melt inclusions vary with host mineral, pumice clast and stratigraphic position (Skirius, 1990; Skirius *et al.*, 1990; Lu, 1991; Lu *et al.*, 1992*a*). Although melt inclusions occur in almost all phenocrysts, they are largest and most abundant in quartz phenocrysts. Except where otherwise noted, the observations summarized below apply to melt inclusions in quartz. Melt inclusions that are larger than about 50 μm are less abundant in late-erupted quartz. Early-erupted inclusions generally are round, whereas late-erupted inclusions commonly are faceted (negative crystal shape). Large, early-erupted inclusions tend to occur near phenocryst rims, whereas most large, late-erupted inclusions are more centrally located. Differences in size and zonal distributions of inclusions probably are primary igneous features and suggest differences in conditions of formation.

Some late-erupted quartz phenocrysts have faceted, clear inclusions located in the interior and round, brown (because of incipient devitrification) inclusions located close to the rim. This zonal arrangement reveals the approximate sequence of inclusion entrapment, and this sequence is important for the interpretation of certain melt inclusion compositional variations given below.

Bubble occurrence and devitrification in melt inclusions correlate with degree of ash-flow welding. Most melt inclusions in the nonwelded plinian pumice-fall deposits are glassy, colorless and bubble free. Melt inclusions from most poorly welded ash-flow pumice contain gas bubbles and range from being brown, because of incipient devitrification, to partly devitrified with micrometre-sized dark crystals. Most large melt inclusions (>50 μm in diameter) from densely welded ash-flow pumice are cracked and have large bubbles; those that remain uncracked are opaque with bumpy outlines, as a result of extensive devitrification and crystallization along the inclusion wall. Larger inclusions are more commonly cracked than small ones, as expected on the basis of stress distribution (Tait, 1992). Inclusions in sanidine are more commonly cracked or burst than inclusions in quartz. Our interpretation is that bubbles and devitrification are mainly the result of relatively slow post-depositional cooling. Our sampling strategy placed a high priority on quartz phenocrysts containing glassy, bubble-free melt inclusions, but some devitrified samples were included for stratigraphic completeness.

COMPOSITIONS OF MELT INCLUSIONS

Sample preparation and analytical methods

Quartz and sanidine phenocrysts with uncracked melt inclusions were hand-picked under a stereo microscope from crystal concentrates immersed in refractive index oil of $n = 1·54$. Selected crystals were positioned in thermal-setting plastic and individually ground so as to expose the largest inclusions on one or both surfaces of the crystal wafer (~ 100 μm thick). Some effort was made to orient crystals for grinding so that multiple inclusions would be intersected, in part to compare inclusions in the core with those near the rim. Selected devitrified inclusions were revitrified before sectioning by heating the host crystals at 800–900°C under ~ 2 kbar of argon gas pressure for 20 h or longer (Skirius *et al.*, 1990). Although the laboratory homogenization apparently affected some CO_2 concentrations, trace element concentrations are similar for both revitrified and naturally glassy inclusions (except for Zr, Ti and perhaps Nb, which apparently resided in crystals that did not completely redissolve upon heating).

Concentrations of major and minor elements were measured with a Cameca SX-50 electron microprobe. To minimize the effect of volatile loss, we used a 30 μm diameter beam size. We first measured Na, K, Si and Al with an energy-dispersive system (EDS) using a 10 nA Faraday-cup current for 10 s, then increased the beam current to 20 nA and used a wavelength-dispersive system (WDS) to measure the minor elements Ca, Fe

and Mg. Trace elements were analyzed with a modified AEI IM-20 ion microprobe. The $^{16}O^-$ primary beam was focused to a 20 µm spot and operated at a beam current of 10–20 nA. Additional details for ion microprobe analyses have been given by Hinton *et al.* (1988), Davis *et al.* (1991) and Simon *et al.* (1991). The data for the Wallace *et al.* (1999) set of melt inclusions were collected with a slightly revised analytical procedure, described by MacPherson & Davis (1994).

Infrared spectrometry (Newman *et al.*, 1986, 1988; Skirius, 1990; Skirius *et al.*, 1990) was used to determine concentrations of H_2O and CO_2 in glass inclusions. Skirius (1990) and Qin (1994) demonstrated that the heating and quenching process used for revitrification leads to an apparent decrease of ~ 0.5 wt % H_2O absolute in inclusions with ~ 6 wt % H_2O. Zhang *et al.* (1997) revised the calibration of the IR molar absorptivities, and this new calibration has been applied to the data reported here with the result that the concentrations of H_2O computed from the IR absorbances are less than those reported by Skirius *et al.* (1990) by up to ~ 0.7 wt %. The precision of the H_2O determinations is better than $\sim 10\%$ relative in nearly all cases, and the principal sources of error are thickness measurement, spectral noise and subjective fitting of background [see Newman *et al.* (1986, 1988) and Skirius (1990)]. The CO_2 determinations followed procedures and used the molar absorptivity of 1078 g/cm per mol at 2350 cm^{-1} established by Blank *et al.* (1989, 1993). Precision of the CO_2 determinations is mostly better than 5% relative, and the detection limit is ~ 5 ppmw for a large, 70 µm thick inclusion.

RESULTS

We analyzed 99 melt inclusions (74 early, one mid and 24 late erupted) for 36 nonvolatile minor and trace elements, and representative analyses are given in Table 1. Of the 24 late-erupted inclusions, seven are also in the dataset of Wallace *et al.* (1999), but are included here because they were analyzed at nearly the same time that we analyzed our other inclusions. We analyzed H_2O and CO_2 in many of the same inclusions as well as in additional inclusions. Our data coverage, and that of Wallace *et al.* (1999), is revealed in our figures and their captions and legends. For clarity, we refer to the data presented here as 'our' data to distinguish them from those presented by Wallace *et al.* (1999). The complete dataset including spectroscopic absorbances, spectral quality, inclusion size and thickness, host mineral, heating (homogenization) history, bubble occurrence and certain other textural notes can be downloaded from the *Journal of Petrology* web site at http://www.petrology.oupjournals.org.

Major element composition

All melt inclusions, whether from early-, mid- or late-erupted Bishop Tuff, in quartz or sanidine phenocrysts, are high-silica rhyolite with ~ 77.6 wt % SiO_2 on an anhydrous basis. Together, SiO_2, Al_2O_3, K_2O and Na_2O make up ~ 99 wt % of the anhydrous total; CaO and FeO account for most of the rest. Early- and late-erupted melt inclusions have similar major element concentrations except for K_2O, which tends to be higher in late-erupted inclusions, as also found by Dunbar & Hervig (1992).

Volatile composition

Modes of dissolved H_2O concentrations in naturally cooled and laboratory heated (and quenched) sets of stratigraphically similar inclusions are similar (Fig. 2), and laboratory heating has no discernible effect on the H_2O concentrations computed using the procedures of Zhang *et al.* (1997). Early erupted inclusions have more H_2O than late-erupted inclusions; however, Wallace *et al.* (1999) showed that mid-erupted inclusions have ~ 0.5 wt % more H_2O than early-erupted inclusions.

Nearly all early-erupted melt inclusions contain relatively low amounts of dissolved CO_2, between 19 and 150 ppm (Fig. 2). Not plotted in Fig. 2 are five mid-erupted, ash-flow-deposited inclusions [Ig2E of Wilson & Hildreth (1997)], which were coarsely devitrified and revitrified completely upon laboratory heating. They lack any textural evidence of leakage. Our five mid-erupted inclusions have H_2O concentrations like those of early-erupted inclusions, but their CO_2 concentrations are dominantly >50 ppm (one has 186 ppm CO_2) in contrast to early-erupted inclusions (almost half of which have <50 ppm CO_2). Other more coarsely devitrified inclusions from other samples evidently leaked through indistinct cracks during devitrification and/or laboratory heating and we exclude their volatile concentrations. The 33 inclusions from the mid-erupted Bishop Tuff analyzed by Wallace *et al.* include seven inclusions with 151–343 ppm CO_2. Our late-erupted inclusions from Aeolian Buttes (location 5, Fig. 1), although revitrified by laboratory heating (Skirius *et al.*, 1990), have high and variable contents of CO_2, ranging from 117 to 761 ppm, similar to stratigraphically comparable but unheated and naturally cooled inclusions from location 6 (Fig. 2) as well as those analyzed from location 6 by Wallace *et al.* (1999) in which CO_2 ranges from 149 to 1085 ppm. With eruptive sequence there is an increase in average CO_2 and a decrease in the proportion of inclusions with <50 ppm CO_2.

Similarly, there is an increase in CO_2 from core to rim for inclusions within some late-erupted crystals. Several late-erupted quartz phenocrysts have clear, faceted inclusions located far from crystal rims and round, brown
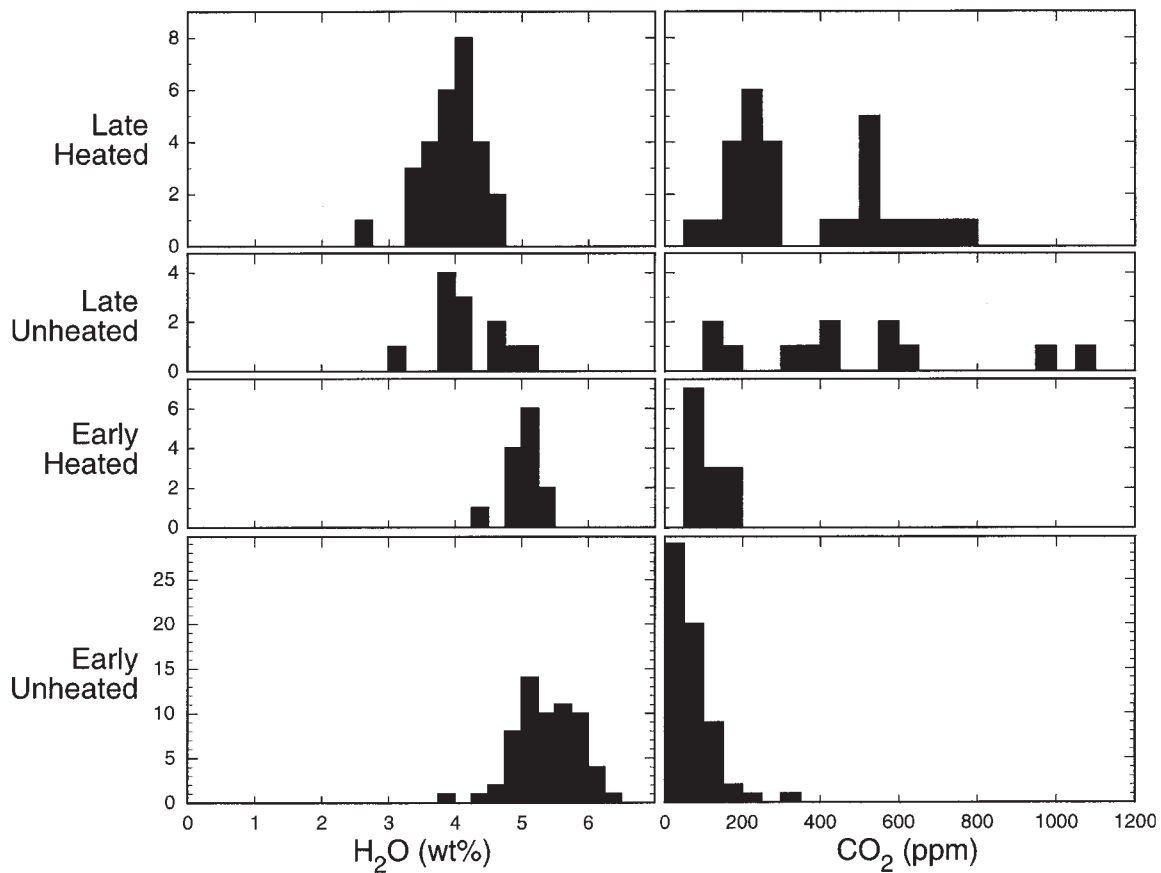
Fig. 2. Histograms of H_2O and CO_2 in melt inclusions, heated and unheated, early and late. Heated and unheated late-erupted inclusions have similar H_2O and CO_2 indicating that heating had a negligible effect on the H_2O and CO_2 in the inclusions and further that the speciation rules of Zhang *et al.* (1997) are appropriate for H_2O at this concentration range. Heated early-erupted inclusions have perceptibly greater CO_2 than unheated early-erupted inclusions, and this is the opposite of expectations if heating were to cause partial loss of CO_2. The difference reflects a sample bias in that most of the heated early-erupted inclusions are from samples having slightly devitrified inclusions, and these are mainly from higher stratigraphic positions compared with most of our early-erupted inclusions. H_2O concentrations are significantly lower, and CO_2 concentrations are substantially higher in late-erupted inclusions. Plotted data are (number of inclusions [sample number abbreviated]): late heated (33 = 9 [17A] + 19 [18A] + 5 [327]); late unheated (12 = 12 [327]); early heated (13 = 4[6B] + 2[10] + 1[13] + 3[16] + 2[21A] + 1[24C]; early unheated (62 = 1[2] + 2[3A] + 2[5B] + 6[5D] + 3[6A] + 7[6B] + 3[7A] + 2[7B] + 1[8A] + 4[8B] + 1[9] + 2[10] + 3[11A] + 3[11B] + 8[13] + 5[15] + 1[16] + 8[21A]). Coarsely devitrified inclusions are excluded because they have incipient cracks and anomalously low CO_2 concentrations and have apparently leaked.

inclusions near the rims of the same crystals (Lu & Anderson, 1991; Wallace *et al.*, 1995; P. J. Wallace, personal communication, 1995). Significantly, the near-rim, round, brown inclusions are relatively high in CO_2 [Fig. 3, and see fig. 4 of Wallace *et al.* (1999)] revealing that, as quartz grew and trapped inclusions of melt, the melt became richer in CO_2. Although CO_2 would increase with crystallization, if no gas were present, the three-fold increase would require 67 wt % crystallization, and a parallel increase in H_2O of only 100% (two-fold) would result in gas saturation at the base of the crust. CO_2

enrichment is the reverse of the effect of *in situ* (closed-system) gas-saturated crystallization.

Trace element composition

Both we and Wallace *et al.* (1999) determined concentrations of trace elements in melt inclusions using the Chicago ion microprobe. The data are compatible, but we use separate symbols for the different sets of data in the figures, because the Wallace *et al.* data were collected
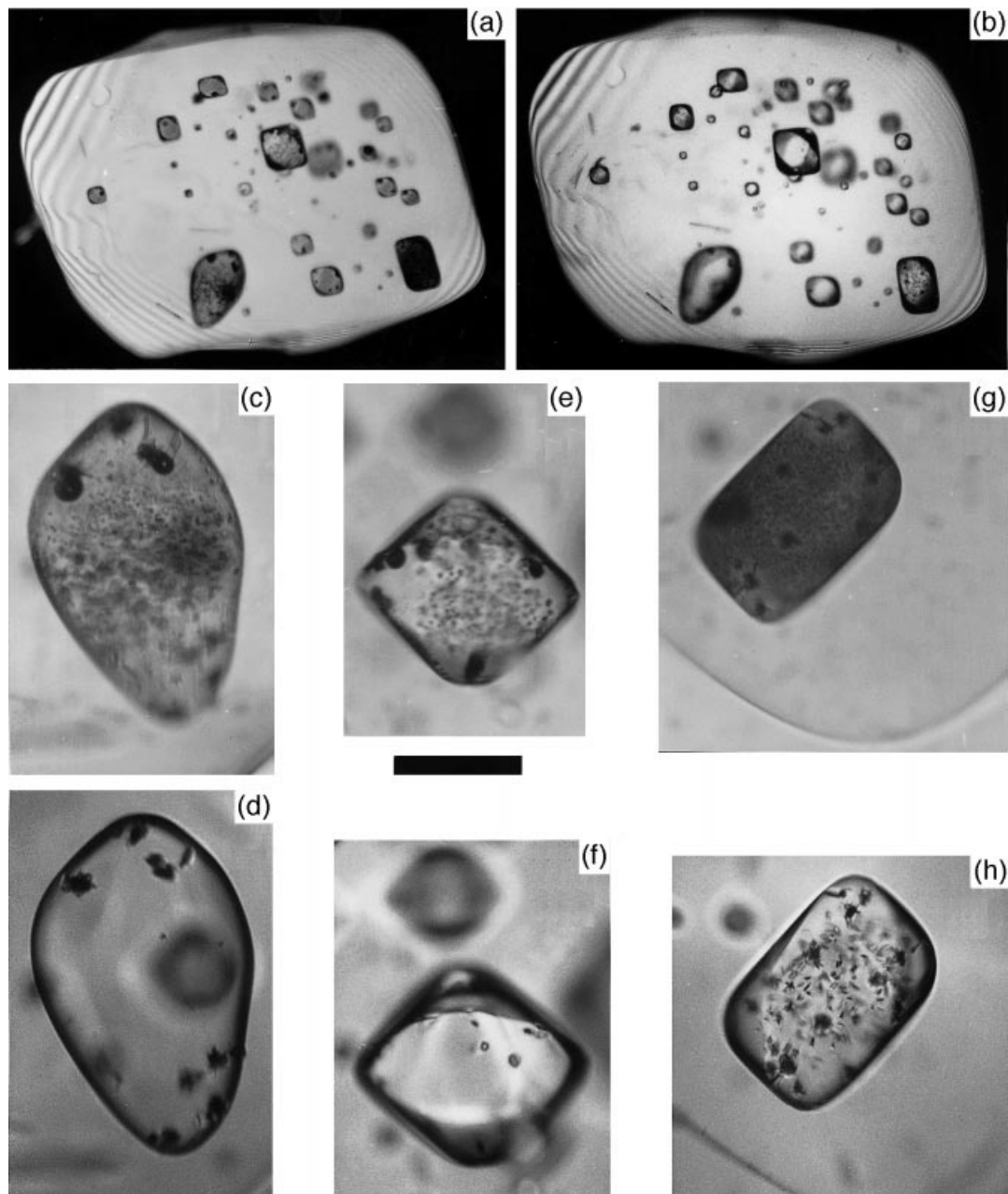
Fig. 3. Photographs of glass inclusions in quartz phenocryst LV81-18A-132 from late-erupted ash flow (location 5). The crystal in (a) and (b) is 1·2 mm long. The scale bar represents 100 μm and applies to (c)–(h). Adhering glass was dissolved using concentrated fluoroboric acid to improve the visibility of the inclusions of glass and to reveal cracked inclusions. (a), (c), (e) and (g) are of the naturally cooled crystal and inclusions. The other views show the crystal and inclusions after 20 h at 800 ± 5°C and ∼2000 bars in an open capsule in an argon gas pressure vessel. In (c) and (e) the inclusions contain small bubbles [round dark circles about 10–30 μm in diameter with tiny bright spots in the middle of the two larger bubbles in (c)]. After heating the bubbles had gone [(d) and (f)] and most devitrification crystals present in (c) and (e) also disappeared, but some larger crystals in radiating clusters remained with little change. Although the brownish, finely devitrified inclusion shown in (a) and (g) became clear upon heating, a number of devitrification crystals coarsened. After sectioning, the heated inclusions shown in (d), (f) and (h) were analyzed spectroscopically for CO_2 and H_2O with the results (CO_2 in ppm and H_2O in wt %) as follows: (d), 710, 4·02; (f) 209, 4·33; (h) 761, 4·70. Errors are roughly 5% relative for CO_2 and 10% relative for H_2O.

with a revised analytical technique (MacPherson & Davis, 1994) that gave slightly higher precision. We focus on only a few of the 36 minor and trace elements determined by ion probe analysis, especially Ba, Sr and Rb, because their behavior is relevant to the relative roles of magma mixing and fractional crystallization; Ba is particularly
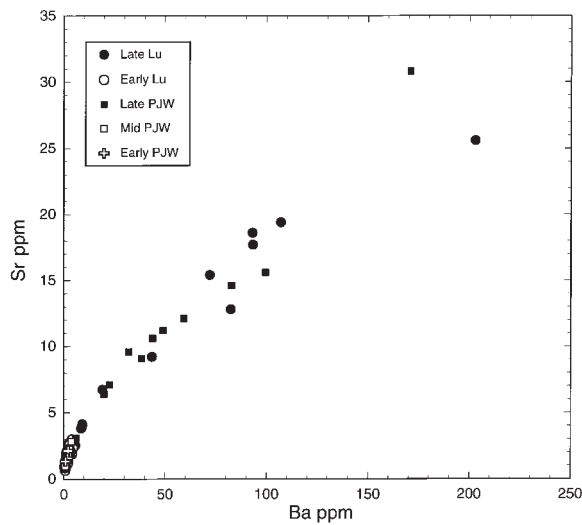
Fig. 4. Concentration of Ba and Sr in melt inclusions. All concentrations are in ppm and are ion microprobe data. Lu data are from this work, PJW are data from Wallace *et al.* (2000). The correlation between Ba and Sr is positive, reflecting the compatibility of Ba in sanidine and of Sr in plagioclase and sanidine. Curvature of the correlation is conspicuous from 0·5 to ∼30 ppm Ba. Uncertainties as a result of 1σ counting statistics are around 0·2 ppm for Sr and 0·5 ppm for Ba, but increase to a few percent relative with concentration. (See text for analytical accuracy.)

Fig. 5. Barium and strontium in melt inclusions plotted logarithmically (same data as in Fig. 4). Compositions of early- and mid-erupted inclusions (open symbols) are indistinguishable. Early- and mid-erupted inclusion compositions overlap late-erupted inclusions (filled symbols) between about 1 and 5 ppm Ba. The straight correlation is tighter for the more recent PJW data and corresponds to an exponential relation such as is expected for fractional crystallization. Ba varies by a factor of ∼400 corresponding to 49 wt % fractional crystallization of a mineral assemblage containing 33 wt % sanidine (sanidine–melt partition factor = 28·4, Lu *et al.*, 1992*b*).

important because of its reversed zonal distribution in Bishop sanidine phenocrysts.

Early-erupted inclusions have uncommonly low concentrations of highly compatible trace elements [especially Ba and Sr, which are concentrated in feldspars; Mg, which is concentrated in mafic minerals; and light rare earth elements (LREE), which are concentrated in allanite]. All early- and mid-erupted inclusions have 4 ppm or less Ba and Sr. Incompatible trace elements [Th, U, Nb, Y, heavy REE (HREE), Rb and Cs, for instance] show small but significant ranges compared with analytical uncertainties. For inclusions in the same early-erupted quartz phenocryst, analyzed inclusions located nearest the rim of the phenocryst have the highest concentrations of incompatible elements (Lu, 1991; Lu *et al.*, 1992*a*). The ranges of incompatible and compatible elements in inclusions from individual early-erupted pumice clasts are consistent with 7 to ∼33 wt % of *in situ* crystallization (Lu *et al.*, 1992*a*; Wallace *et al.*, 1995).

Late-erupted inclusions have trace element compositions that range from those of the early inclusions to roughly four-fold lower concentrations of incompatible elements (e.g. U, Th, Rb, Cs, Y, HREE) and to roughly 100-fold greater concentrations of compatible trace elements [e.g. Ba and Sr (Figs 4 and 5)]. The much greater range of variation for compatible as compared with incompatible elements is expected for differentiation caused by fractional crystallization.
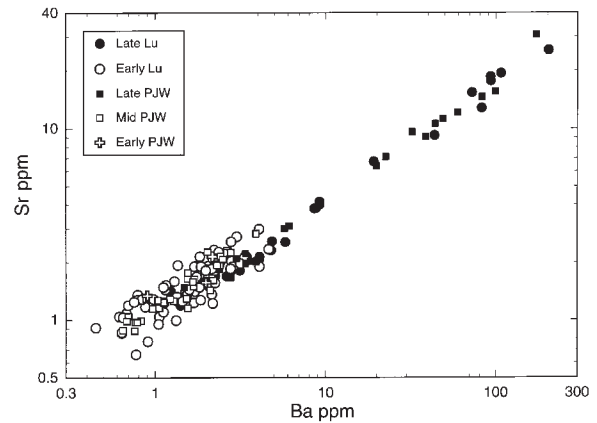
Most element–element correlations show significant overlap between early- and late-erupted inclusions, and such overlap is consistent with Hildreth's (1979) whole-rock data and his interpretation that the Bishop magma body was continuous, but zoned. Correlations of Mg with Ca largely separate our late- from early-erupted inclusions. However, our samples reflect only part of the stratigraphic sequence, and it is possible that overlap in Mg vs Ca exists in melt inclusions in parts of the deposits that we have not analyzed.

Ba (concentrated in sanidine) and Sr (concentrated in plagioclase and sanidine) are highly compatible, and they define a tight correlation that is linear on a log–log plot (Fig. 5) over a range of a factor of 400 in Ba concentration. This correlation is discussed in detail below.

There is an overall positive correlation between CO_2 and Ba (Fig. 6), particularly at higher concentrations of Ba characteristic of late-erupted inclusions. This correlation is similar for both bubble-bearing and bubble-free melt inclusions, implying negligible residence of CO_2 in most bubbles. Therefore, the correlation mainly reflects intrinsic variations in CO_2 dissolved in the melt from which the crystals grew. It is, thus, petrologically important that CO_2 concentrations are noticeably scattered [compare, for example, the CO_2 vs Ba plot (Fig. 6) with the Ba vs Sr plots (Figs 4 and 5)]. The probable explanation of greater scatter in the concentrations of CO_2 as compared with nonvolatile elements is that the inclusions formed from polybaric gas-saturated magma that exsolved variable proportions of CO_2.
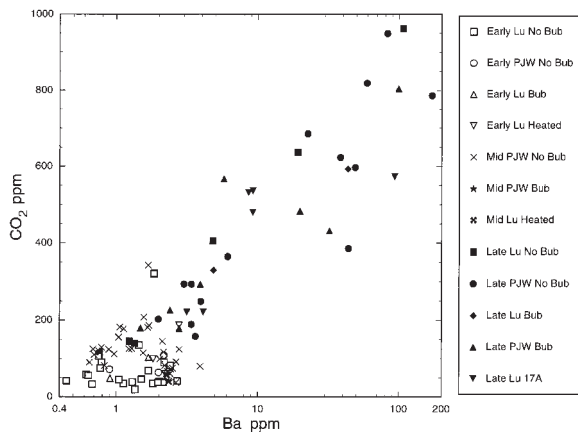
Fig. 6. CO_2 and Ba in early-, mid- and late-erupted melt inclusions. Bubble-bearing ('Bub' in legend) inclusions are similar to bubble-free ('No Bub' in legend) inclusions consistent with negligible or minor amounts of low-density CO_2 in relatively small bubbles. CO_2 generally increases with Ba, especially for the Ba-rich, late-erupted Bishop inclusions. Data of Wallace *et al.* (2000) (PJW) are plotted together with the data of this work (Lu). Eleven inclusions are not plotted, because they were completely devitrified, have incipient cracks and required repeated heating for homogenization, and all yielded CO_2 concentrations <150 ppm.

Some inclusions in late-erupted quartz phenocrysts are compositionally compatible with formation from early-type magma on the basis of similar K_2O, CO_2, Ba, Sr and Rb concentrations. However, in all of these cases, the CO_2, Ba and Sr concentrations are in the upper part of the range for early-erupted inclusions. One such inclusion is from a unique clast (327-3-5) that lacks pyroxene and contains other inclusions that have both high H_2O (like early-erupted inclusions) and high CO_2 (like late-erupted inclusions). Preeruptive transfer of some quartz phenocrysts from early-type magma into the late-erupted, pyroxene-phyric magma is a possibility.

Comparison with the data of Dunbar & Hervig (1992)

Our data on melt inclusions are in general agreement with those of Dunbar & Hervig (1992). In detail, our ion probe analyses for some elements (e.g. B and Rb) show less overlap between early- and late-erupted inclusions (Fig. 7). Our analyses of H_2O are much more tightly grouped than are those of Dunbar & Hervig (1992). The differences probably reflect a combination of differences in sample preparation (we excluded cracked inclusions and reentrants), sample inventory and analytical precision. Our interpretations differ from those of Dunbar & Hervig (1992) in part because of the tighter arrays of our data.

Gas-saturation pressure

Gas-saturation pressures are the static pressures that a melt would be under if it were saturated with gas and in equilibrium with a separate gas phase. Gas-saturation pressure is the minimum possible equilibrium pressure that a melt was under. If the melt were not gas saturated, then its static pressure would be higher than the gas-saturation pressure. Gas-saturation pressure is calculated based on the inferred igneous temperature and observed concentrations of volatile components dissolved in the melts. The solubilities of volatiles dissolved in a melt increase with increasing gas pressure and decrease slightly with rising temperature.

The gas-saturation pressures of the melt inclusions were calculated based on their H_2O and CO_2 concentrations using a fit of solubility data (Burnham & Jahns, 1962; Silver *et al.*, 1990; Blank *et al.*, 1993) devised by Wallace (Wallace *et al.*, 1995, 1999). Temperatures of 725°C and 790°C were assumed, following Hildreth (1977, 1979), for early-erupted (including mid-erupted samples 133) and late-erupted inclusions, respectively. Representative results are given in Table 1 and the complete data are available in the electronic appendix. There is a large overlap in gas-saturation pressures between our early- and late-erupted melt inclusions: 1·0–2·3 kbar for the early-erupted and 1·1–3·0 kbar for the late-erupted inclusions. Our gas-saturation pressures are similar to those reported by Wallace *et al.* (1999), who discussed these data in detail. Here we focus on the rimward increase in gas-saturation pressures of inclusions within some single, late-erupted quartz phenocrysts (e.g. crystal LV-18a-132, Fig. 3).

COMPOSITIONS OF FELDSPAR PHENOCRYSTS

Plagioclase

Plagioclase phenocrysts in the early-erupted Bishop Tuff are compositionally uniform at about $An_{15}Ab_{78}Or_7$. Those from the late-erupted Bishop Tuff, however, show a wide range of compositions (An_{13-48}) with the majority falling into the range of An_{19-25}. The rims of analyzed late-erupted plagioclase phenocrysts (about 60 grains) are $An_{21-23}Ab_{69-70}Or_{7-8}$, about 10% have a more calcic core ($An_{32-48}Ab_{50-64}Or_{3-4}$) and another 10% have a more sodic core indistinguishable from those of the early-erupted Bishop Tuff (Lu, 1991).

Sanidine

Sanidine phenocrysts from the early- and late-erupted Bishop Tuff are identical with respect to major elements ($Ab_{33-35}Or_{64-66}An_{<1}$ and $Ab_{32-35}Or_{65-67}An_{1-2}$, respectively). In terms of major elements, analyzed sanidine phenocrysts are uniform.
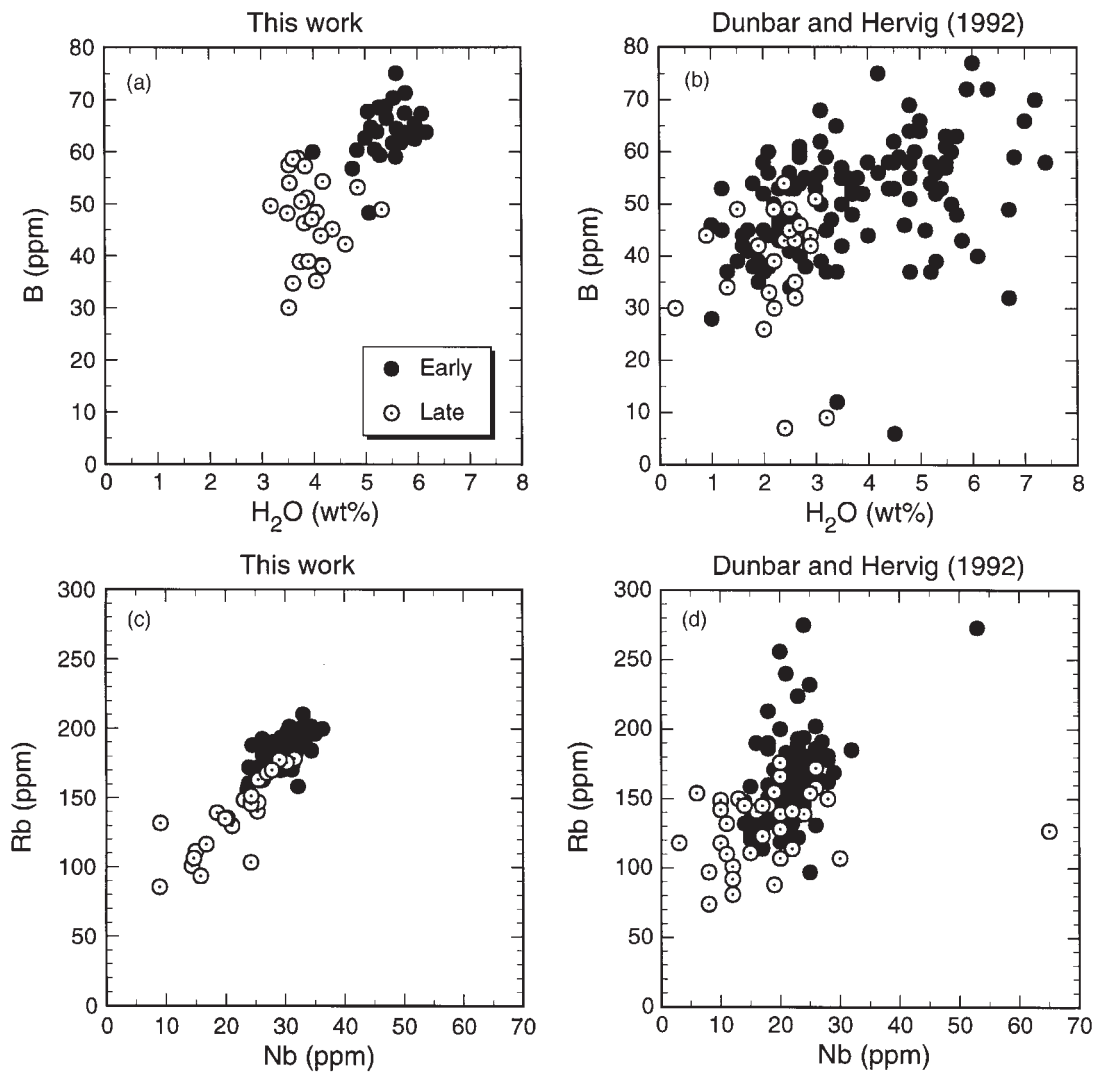
Fig. 7. Comparison of our data with those of Dunbar & Hervig (1992). Both datasets cover similar ranges and show qualitatively consistent differences between early- and late-erupted inclusions. Our data cluster more tightly, and the close coherence between incompatible elements such as Rb and Nb helps constrain plausible mechanisms of differentiation. However, the scatter in our data still exceeds that based on counting statistics alone.

However, trace element abundances in sanidine vary. Early-erupted sanidine phenocrysts are extremely poor in Ba and Sr. Barium is below the electron microprobe detection limit of 200 ppm (Lu, 1991) in all 20 early crystals analyzed by electron microprobe. Ion microprobe analyses of six crystals range from 24 to 70 ppm Ba and from 13 to 32 ppm Sr. Detailed ion microprobe traverses of five early-erupted sanidine phenocrysts by Dunbar & Hervig (1992) revealed that Ba and Sr concentrations in early-erupted sanidine phenocrysts decrease slightly or remain constant from core to rim.

Mid- and late-erupted analyzed sanidine phenocrysts are reversely zoned with respect to Ba, Ca and Fe. The extent of zoning is variable. Sanidine phenocrysts from our mid-erupted Tableland samples (Ig2E of Wilson & Hildreth, 1997) increase in Ba more than ten-fold from <180 ppm in the core to ~2200 ppm at the rims (Fig. 8). Ca and Fe also increase toward the rims. All 30 analyzed sanidine fragments from our Mono ash-flow lobe samples (Ig2NW of Wilson & Hildreth, 1997) show more extreme Ba zonation from below 180 ppm Ba at the core to ~8900 ppm Ba at the rims (Fig. 8). Again, Fe and Ca are similarly zoned. Ion microprobe analyses of one late-erupted sanidine phenocryst reveal that concentrations of compatible elements (Ba, Sr, La and Ce) increase, whereas Rb (incompatible) decreases towards the rims (Fig. 9). Two-dimensional images of Ba, Fe, Rb and K in a late-erupted sanidine phenocryst obtained
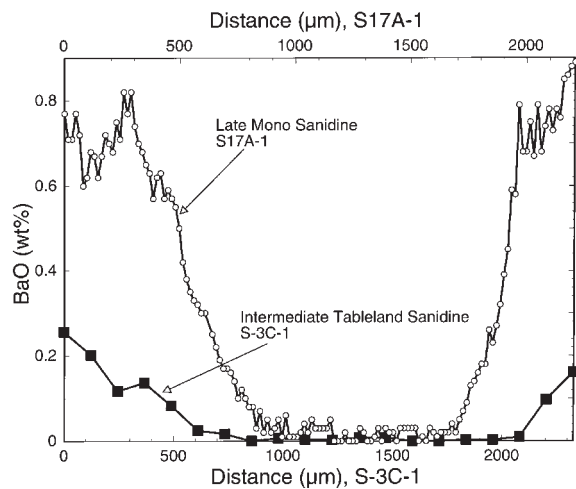
Fig. 8. Ba zonation in late- and mid-erupted sanidine phenocrysts determined by electron microprobe. It should be noted that Ba (a highly compatible or captured element in sanidine) increases towards the rims. The rim of the sanidine phenocryst from Tableland ash-flow lobe (Ig2E of Wilson & Hildreth, 1997) has ∼0·25 wt % BaO, whereas the rim of the sanidine phenocryst from Mono ash-flow lobe (Ig2NW) has up to ∼0·9 wt % BaO (a portion of the crystal rim may be missing because of fracture). Oscillatory zoning of BaO is evident on the left side of the Mono sanidine. Analytical uncertainty corresponding to 1σ counting statistics is ∼0·02 wt %.

Fig. 9. Trace element zonation in a late-erupted sanidine phenocryst, determined by ion microprobe. Concentrations of compatible Ba, La, Ce and Sr increase, whereas the concentration of incompatible Rb decreases slightly from the core to the rims of the crystal. The zonation of Ba is much greater than that of Sr. Analytical precision is as mentioned in Fig. 4 for Ba and Sr and about 3 ppm for Rb, 2 ppm for Mg, 0·2 ppm for La and 0·7 ppm for Ce.

with the synchrotron X-ray fluorescence microprobe at Brookhaven National Laboratory indicate that the concentrations of both Ba and Fe increase towards the rim of the crystal, and that superimposed on the overall zonation there are correlated oscillatory zonings of Ba and Fe (Lu, 1991). Thus the Ba and Fe zoning appears to reflect crystallization rather than diffusion.

We emphasize that the zonation of Ba in sanidine is consistent with the zonation of CO_2 in melt inclusions in quartz, in view of the positive correlation between Ba and CO_2. Thus, both quartz and sanidine phenocrysts from the late-erupted Bishop Tuff evidently grew from liquids that were increasingly Ba and CO_2 rich.

The Ba concentration in the interior of a late-erupted sanidine phenocryst is 116 ppm (Fig. 9), which is only a factor of two higher than those of some early-erupted sanidines (24–70 ppm, Lu, 1991). This is consistent with the Ba concentrations in early-erupted melt inclusions in quartz using the sanidine–melt partition factor of 28·4 for Ba (Lu *et al.*, 1992*b*).

The Sr concentration (∼200 ppm) in the core of the late-erupted sanidine phenocryst (Fig. 9) is, however, almost a factor of eight greater than those of the early-erupted sanidine phenocrysts. This Sr concentration is much higher than that expected for sanidine in equilibrium with early-erupted melt inclusions, using the sanidine–melt partition factor of 11 for Sr (Lu *et al.*, 1992*b*).
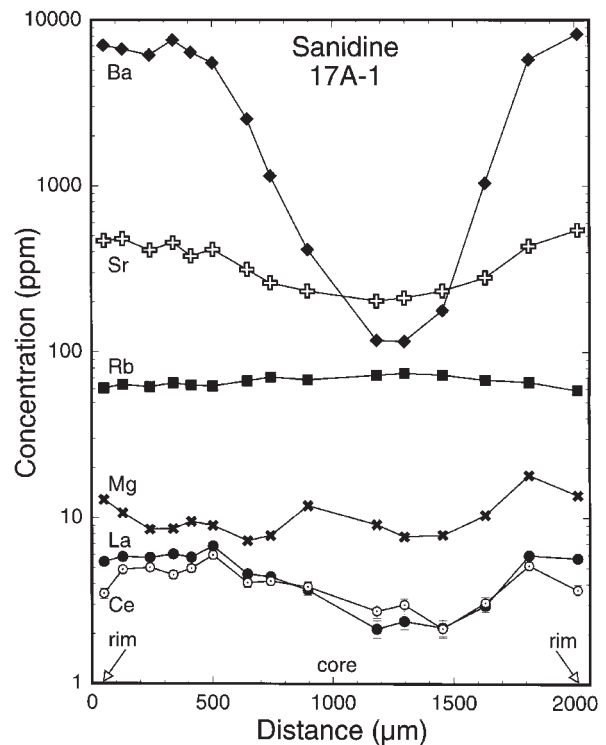
COMPOSITION OF MAGNETITE

Crystals of magnetite occur as independent (solitary) phenocrysts and as inclusions in other phenocrysts. Individual unaltered magnetite phenocrysts throughout the Bishop Tuff are compositionally unzoned (Hildreth, 1979). Magnetite phenocrysts from various early-erupted Bishop samples vary over a comparatively small but significant range with respect to Fe and Ti, regardless of depositional subunit. For the entire Bishop Tuff, the variations of Fe and Ti concentrations in magnetite are small, but Mg, Al and V increase and Mn decreases significantly with higher magnetite–ilmenite equilibration temperatures (Hildreth, 1977, 1979).

Figure 10 shows MnO and Al_2O_3 vs MgO for both the magnetites of this study and the results of Hildreth (1977). Our gap at the intermediate compositions may reflect a lack of unaltered magnetite phenocrysts in our Tableland (Ig2E) pumice samples. The solitary late-erupted magnetite phenocrysts define a group characterized by relatively high concentrations of MgO (and Al_2O_3 and V_2O_3) and relatively high magnetite–ilmenite equilibration temperatures (Hildreth, 1979).
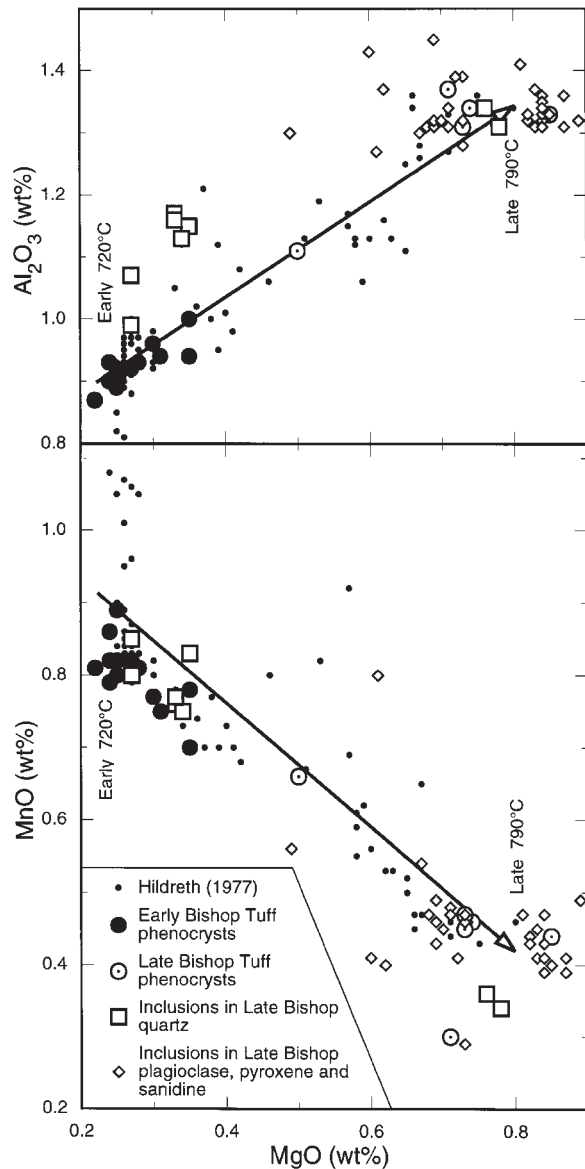
Fig. 10. MnO and Al_2O_3 vs MgO in magnetite crystals. The compositional data and temperature trend of Hildreth (1977, 1979) are shown for comparison. Compositions of included crystals largely overlap those of non-included phenocrysts. However, six out of eight included magnetite crystals in late-erupted Bishop quartz phenocrysts have lower MgO and higher MnO concentrations than the non-included late-erupted Bishop magnetite phenocrysts; they are similar to the non-included early-erupted Bishop magnetite phenocrysts. Inclusions of magnetite in phenocrysts of other late-Bishop minerals are compositionally similar to non-included late-Bishop phenocrysts of magnetite. These features reveal that the late-erupted Bishop crystals contain at least two texturally and compositionally distinct populations of magnetite.

Inclusions of magnetite in late-erupted Bishop phenocrysts, however, comprise two distinct groups. One is similar to that of the solitary phenocrysts with high Mg, Al and V, and low Mn contents. This group includes

two of the eight analyzed magnetite inclusions in quartz and all 33 analyzed magnetite inclusions in plagioclase, sanidine and pyroxene phenocrysts. The other group consists of six of the eight analyzed magnetite inclusions in quartz phenocrysts (Fig. 10). These six magnetite inclusions have low Mg, Al and V, and high Mn contents, and are similar to early-erupted magnetite phenocrysts.

DISCUSSION

We focus our discussion on three topics: (1) origin of the highly differentiated rhyolite; (2) crystal settling vs magma mixing; (3) ages of differentiation, crystallization and the duration of magma storage.

Origin of the high-silica rhyolite of early-erupted Bishop Tuff

The highly differentiated early-erupted Bishop magma had a major element composition that was the same for the bulk rock, matrix glass and melt inclusions, as expected for a eutectic system. Rocks having eutectic compositions, such as the Bishop Tuff rhyolite, plausibly originated either by partial melting or crystallization differentiation or both.

The roles of fractional crystallization and partial melting can be evaluated by considering Sr and Ba in the early-erupted Bishop Tuff. Halliday (1990) and others have argued that the exceptionally low Sr content, 0·1 ppm, in early rhyolites from Glass Mountain requires fractional crystallization. Early-erupted Bishop melt inclusions have 0·5–2 ppm Sr (the bulk rocks including 10% feldspar phenocrysts would have about 1–4 ppm Sr). Using a bulk crystals–melt partition coefficient for Sr of seven (explained below) instead of two (Halliday, 1990) the most differentiated Bishop magma ($\sim$2 ppm Sr) might be derived by first 10% partially melting a source gneiss with 600 ppm Sr yielding a melt with 93 ppm Sr, followed by about 50% of fractional crystallization. Isotopic data for Sr reveal, however, that most of the Sr must derive from young and/or Rb-poor (e.g. basaltic) sources (Halliday *et al.*, 1984; Christensen & DePaolo, 1993). For barium the bulk crystals–melt partition coefficient is 12·6 (explained below). The majority of crustal rocks have K-feldspar with >500 ppm Ba (Puchelt, 1972). A hypothetical 10% partial melt of a granitoid source rock, which initially contained 40 wt % potassium feldspar with 500 ppm Ba, would have $\sim$17 ppm Ba. A decrease in Ba concentration in magma from 17 ppm to 5 ppm Ba (for the most differentiated Bishop magma) requires only $\sim$10% of the original magma to fractionally crystallize as the Bishop phenocryst assemblage. Thus partial melting followed by modest

amounts of fractional crystallization suffice to explain the low concentrations of Sr and Ba in the Bishop magma.

Crystal settling (sinking) and/or magma mixing

We now reassess the roles of crystal settling [rejected, for compelling reasons, by Hildreth (1979)] and magma mixing [proposed by Lu & Anderson (1991) and Hervig & Dunbar (1992)] in the Bishop magma body. The reasoning, in skeletal outline, is as follows:

(1) the reversed zoning of the sanidine phenocrysts indicates that late-erupted sanidine crystals grew from melt that became progressively less differentiated (richer in compatible Ba) with time. Either Ba was added to the melt (by magma mixing or from some contaminant) or the crystals moved into successively more Ba-rich melt (crystal sinking could do this).

(2) Melt inclusions in quartz phenocrysts have a zonal aspect marked by CO_2-rich melt inclusions located preferentially closer to crystal rims, indicating an enrichment in CO_2 with crystallization. This zonation is compatible with the Ba-rich rims of the sanidine phenocrysts, because Ba and CO_2 are positively correlated in late erupted melt inclusions.

(3) As explained below, relations between Ba, Sr and Rb in late erupted melt inclusions are difficult to reconcile with magma mixing, but consistent with fractional crystallization, although in reverse.

(4) Near-rim, late-erupted CO_2-rich melt inclusions have relatively high gas-saturation pressures consistent with substantial increase in pressure during growth and entrapment of melt inclusions. Crystal sinking could cause this.

In conclusion, we require either magma mixing or crystal sinking or both. As discussed below there is a problem with mixing, and there is significant support for sinking. Thus we conclude that at least some late-erupted crystals sank into progressively less differentiated melt as they grew. Some detailed aspects of the above skeletal argument are elaborated below.

It is important, but not yet possible, to establish whether the late-erupted Bishop magma was gas saturated during phenocryst growth. The large variation in the ratio (ppm CO_2)/(wt % H_2O) from 40 to >200 (Fig. 11) for late-erupted melt inclusions is suggestive of gas-saturated crystallization. Such large variations can easily occur in a gas-saturated magma, because isobaric crystallization of volatile-poor minerals causes gas to exsolve and preferentially deplete the melt in relatively insoluble CO_2 (yielding residual melt with a decreased ratio of dissolved CO_2/H_2O). CO_2 varies by more than a factor of five, and it is difficult to see how such a large variation could arise in the absence of gas saturation.
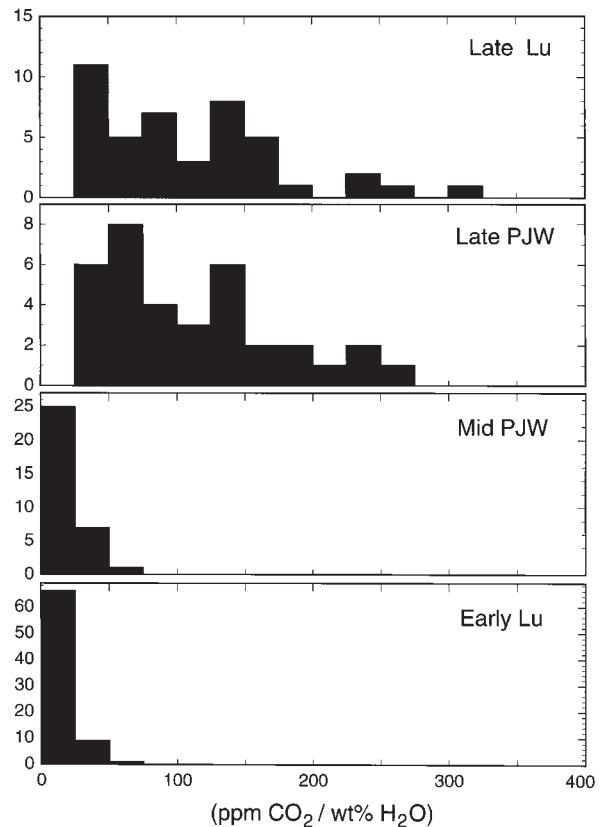

Fig. 11. Ratios of dissolved CO_2 to H_2O in early-, mid- and late-erupted melt inclusions [expressed as (ppm CO_2)/(wt % H_2O) = 10 000 × mass concentration ratio of CO_2/H_2O]. Data plotted are for both heated and unheated inclusions from Wallace *et al.* (2000) ('PJW') as well as this work ('Lu'). The CO_2/H_2O ratios are indistinguishable for early- and mid-erupted inclusions. There is only a little overlap with the generally higher CO_2/H_2O ratios of late-erupted inclusions. The CO_2/H_2O ratio varies by about a factor of 10 for early-, mid-, and late-erupted inclusions and requires a process such as gas-saturated differentiation that can separate CO_2 from H_2O. Data plotted include early- and late-erupted inclusions analyzed by Lu (our data) and mid- and late-erupted inclusions analyzed by Wallace *et al.* (2000). The datasets are similar both for the early Lu and mid Wallace as well as the late Lu and late Wallace. (Note that there are more than twice as many inclusions in the early Lu dataset compared with the mid Wallace data.)

Wallace *et al.* (1999) suggested that all late-erupted inclusions initially formed at 2·5–3 kbar with a substantial range in H_2O as well as in CO_2 and CO_2/H_2O ratios reflecting gas-saturated crystallization. Possible diffusive loss of some H_2O from relatively H_2O-rich, CO_2-poor inclusions would increase the range of gas-saturation pressures. Lack of bubbles in some late-erupted melt inclusions from the Crestview samples (location 6), and the presence of only very small bubbles in others suggests that loss of H_2O was limited, however. Thus we think the range in gas-saturation pressures closely reflects the original range of pressures of formation of the inclusions.

We interpret some of the features described above in terms of a hypothetical precursor magma that moved into the upper parts of the magma body. The evidence for such a precursor lies in: (1) the cores of some late-erupted sanidine phenocrysts, which are relatively Ba poor like early-erupted sanidine phenocrysts; (2) the six magnetite inclusions in late-erupted quartz that have compositions like early-erupted magnetite; (3) a few late-erupted melt inclusions that are compositionally similar to early-erupted inclusions (Figs 5 and 6). Inclusion 18A-132-3 (Fig. 3, and see the electronic appendix) in the interior of crystal 132 has a modest CO_2 content of 209 ppm and may best represent the initial composition of this hypothetical precursor magma. We stress that these attributes are not identical with those of the early-erupted magma, but it is our hypothesis that such a precursor magma existed during an early evolutionary stage of the Bishop magma body and that these features are relics contained in phenocrysts that sank out of the upper parts of the precursor magma as it evolved to become the early-erupted magma.

The concentrations of compatible elements in magma provide sensitive tests of differentiation processes, because any given increment of fractional crystallization can yield far greater variations for compatible elements than for incompatible elements. The partition coefficient for Ba between sanidine and rhyolitic melt is very large (28·4) and, as sanidine is a major crystallizing mineral, the bulk partition coefficient between the crystallizing minerals and the melt is also very large. Therefore, we expect large variations in Ba concentration if fractional crystallization occurs. We observe that Ba varies by a factor of ~ 200 in melt inclusions compared with a factor of less than two for incompatible U. Although this observation is highly suggestive of fractional crystallization, we evaluate below whether the observed variation may reflect mixing between more and less fractionally differentiated end-member melts.

The nature of the differentiation process can, in part, be evaluated based on the detailed form of correlations between compatible elements. Here we scrutinize the relations between Ba and Sr because both are compatible in feldspars. Plagioclase and sanidine are dominant phenocryst minerals whose relative proportions and major element compositions are approximately fixed by the eutectic nature of the rhyolitic magma. Neither Ba nor Sr are fixed in this way and both should vary widely if governed by fractionation. Furthermore, the concentration of Ba should be exponentially related to that of Sr through the difference in their bulk partition coefficients. Thus the logarithm of Ba should be a linear function of the logarithm of Sr with the slope being governed by the partition coefficients. The slope will remain the same as long as the bulk partition coefficients remain the same, which is expected for the Bishop

rhyolitic magma, because it approximated a eutectic system for major elements. Therefore, the slope of the relation between the logarithms of Ba and Sr should remain unchanged or little changed over wide ranges in Ba concentration, if fractional crystallization is the process causing variation.

Mixing together of end-member liquids, on the other hand, is a linear process, and the logarithm of Ba would not, in general, be a linear function of the logarithm of Sr. If the range of variation were small, as it is for incompatible elements, it would be difficult, in view of analytical uncertainties, to distinguish between a linear and exponential array. The large observed range in Ba and Sr concentrations in melt inclusions provides a sensitive test of whether the variations largely reflect an exponential process such as fractional crystallization or a linear mixing process.

To further enhance the sensitivity of our test we have examined the ratios Ba/Rb and Sr/Rb and their logarithms. Dividing both Ba and Sr by Rb helps in two ways: (1) it minimizes scatter caused by instrumental drift because Ba, Sr and Rb have similar small day-to-day variations in ion yield during ion microprobe analysis; (2) as Rb is moderately incompatible in the Bishop phenocryst assemblage (less than $\sim 2\%$ biotite) it will tend to increase with fractional crystallization whereas Ba and Sr will decrease. Thus the ratios will change somewhat more than the absolute mass concentrations, further increasing the sensitivity of the test. Algebraic manipulation of the differential equation for fractionation (for example),

$$\partial \log(Ba) = (D_{Ba} - 1)\partial \log f \qquad (1)$$

yields the following expression for the slope of the changes in Ba/Rb vs Sr/Rb:

$$\frac{\partial \log(Ba/Rb)}{\partial \log(Sr/Rb)} = \frac{(D_{Ba} - D_{Rb})}{(D_{Sr} - D_{Rb})} \qquad (2)$$

where Ds are bulk crystal–liquid partition coefficients and f is mass fraction of liquid remaining.

Figure 12 shows our data and those of Wallace *et al.* (1999) in terms of the logarithms of Ba/Rb and Sr/Rb. We have fitted two lines to the data, one for all early- and mid-erupted inclusions and another for all late-erupted inclusions. The two lines differ slightly but significantly, plausibly reflecting a slightly greater proportion and/or Ca content of plagioclase for the late-erupted crystallizing mineral assemblage. We independently predicted the slope of the relation by assessing the terms on the right side of (2) using our sanidine–melt partition factors and assuming the eutectic condition such that the proportions of sanidine, plagioclase and biotite in the crystallizing mineral assemblage are those required to maintain constant K_2O (for sanidine) and CaO in the
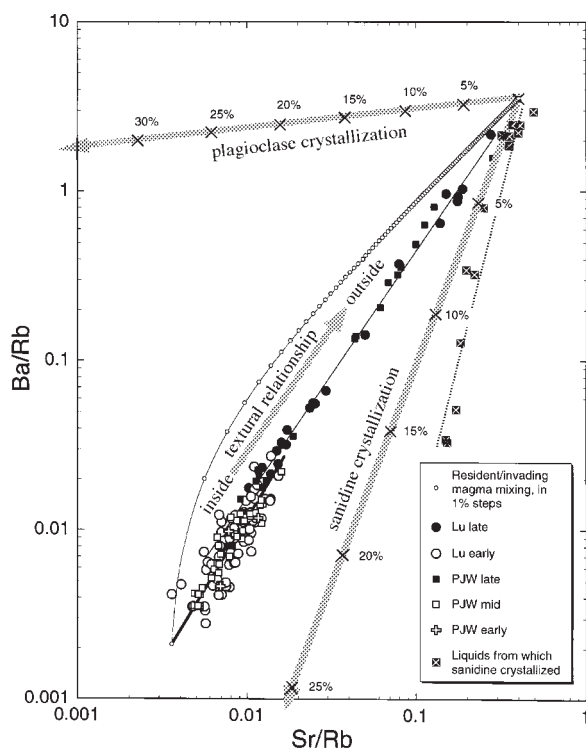
Fig. 12. Log(Ba/Rb) vs log(Sr/Rb) for melt inclusions. A weighted regression of log(Ba/Rb) vs log(Sr/Rb) with each data point weighted by its uncertainties in each direction gave slopes of 1·673 ± 0·063 for the early- and mid-erupted inclusions and 1·460 ± 0·008 for late-erupted inclusions. Two bold arrows show the sense and magnitude (5 wt % tick marks) of the effects of fractional crystallization of sanidine (slope is 2·60 based on sanidine–melt partition factors for Ba, Sr and Rb of 28·4, 11·3 and 0·59) and plagioclase (slope is 0·11 based on plagioclase–melt partition factors for Ba, Sr and Rb of 1·7, 14·6 and 0·084). The observed correlation for the early- and mid-erupted inclusions corresponds to fractional crystallization of a mineral assemblage containing 2·18 times as much sanidine as plagioclase, compared with observed 3:1 ratio of sanidine to plagioclase. For the late-erupted inclusions, the calculated sanidine to plagioclase ratio in the crystallizing assemblage is 1·52. The textural relationship arrow in the middle of the graph reveals that the observed zonation of sanidine phenocrysts is opposite in sense to that expected to result from fractional crystallization. Mixing two end-member melts (see text) yields a non-linear relationship and is shown as a series of small open circles connected by a curved line. A process of mixing followed by fractional crystallization would trace a zig-zag pattern up from the slope 1·67 observation line toward a point on the mixing curve and then back down to the observation line along a slope 2·60 line parallel to the sanidine crystallization line and so forth. Such a process can fit the observations, but is arbitrary and raises quantitative problems, as explained in the text. The compositions of liquids from which the late-erupted, zoned sanidine crystal 17A-1 (Fig. 8) would have formed are shown as filled-box crosses. (Note that only the most Ba- and Sr-rich melt inclusions are compatible with the sanidine crystal and then only with its Ba-rich rim.)

melt (for plagioclase). We assumed Ba enters sanidine only, Sr enters sanidine and plagioclase, and Rb enters biotite and sanidine.

The relevant values are: for sanidine, $D_{Ba} = 28·4 ± 4·1$, $D_{Sr} = 11·3 ± 0·7$ and $D_{Rb} = 0·593 ± 0·008$; for

plagioclase, $D_{Ba} = 1·69 ± 0·37$, $D_{Sr} = 14·6 ± 2·1$ and $D_{Rb} = 0·084 ± 0·040$; and for biotite, $D_{Ba} = 7·1 ± 2·7$, $D_{Sr} = 0·063 ± 0·028$ and $D_{Rb} = 1·43 ± 0·25$. Sanidine–melt partition coefficients are from the data of Lu (1991). For plagioclase, we used the partition coefficient parameterizations of Blundy & Wood (1991) for Sr and Ba, assuming 750°C and An_{15}. Their compilation of literature data covers the entire range from albite to anorthite, but the values at the albitic end are based on rhyolitic melts. For Rb in plagioclase, we used the parameterization of Bindeman *et al.* (1998). This parameterization is based on partitioning between plagioclase and basaltic andesite composition melt and only extends down to An_{40}, so we used it only for Rb. For biotite, we used some of our unpublished data on coexisting biotite and K-feldspar in granulites and amphibolites to calculate biotite–sanidine partitioning and then used the Lu (1991) sanidine values to calculate the biotite values. The proportions of sanidine and plagioclase were chosen such that the melt had the same K_2O and CaO contents, respectively; the proportion of biotite is from Hildreth (1977); quartz makes up the remainder. Using proportions of 40·1% quartz, 42·9% sanidine, 15·0% plagioclase and 2% biotite, we obtain the following bulk partition coefficients: $D_{Ba} = 12·6 ± 1·8$, $D_{Sr} = 7·04 ± 0·44$ and $D_{Rb} = 0·296 ± 0·009$. The resulting value for the right side of equation (2), the slope on a log(Ba/Rb) vs log(Sr/Rb) plot, is 1·82 ± 0·29, where the uncertainty reflects uncertainties in partition coefficients. The slope is sensitive to the sanidine/plagioclase ratio, so uncertainty in this ratio adds to the total uncertainty in the slope. The slopes of weighted regressions through the data in Fig. 12 (late, 1·460 ± 0·008; early and mid, 1·673 ± 0·063) are within the range of our predicted slope. These regressions were calculated by weighting each point by its uncertainty in Ba/Rb and Sr/Rb, according to the method of Williamson (1968). The sanidine/plagioclase ratio in the crystallizing assemblage used in the calculation above is 2·86. To match the slope of late melt inclusions, the sanidine/plagioclase ratio would have to be 1·52; for the early and mid melt inclusions, the ratio would have to be 2·18. The observed relations are consistent with fractional crystallization.

Binary mixing of a differentiated melt (Ba = 0·389, Sr = 0·664, Rb = 186 ppm; slightly below the low end of Fig. 12) with a less differentiated melt (Ba = 330, Sr = 37·4, Rb = 93·4 ppm; slightly above the high end) is shown for comparison, and the mixed compositions lie off the data array by far more than our analytical errors allow. If we consider separately the early–mid and late segments of the correlation, the case for mixing remains weak: the fit of the data to two linear mixing lines yield early–mid and late correlation coefficients (R^2) of 0·71 and 0·95, respectively, whereas two log–log lines are better, with $R^2 = 0·74$ and 0·99, respectively. Binary

mixing does not fit our data, but fractional crystallization does. However, the senses of zoning of both the sanidine phenocrysts and the melt inclusions in phenocrysts are opposite to those predicted by fractional crystallization! Mixing can explain the sense of the zoning, but not the form of the correlation. Fractional crystallization can explain the form of the correlation but not the sense of the zoning!

We considered a combination of binary mixing (as above) followed by fractional crystallization of sanidine. There are three problems with such a scenario:

(1) it must be assumed that, following each increment of mixing, sanidine crystallizes but quartz does not, as there are no melt inclusions in quartz with compositions between the mixing line and the data.

(2) The amount of sanidine that must crystallize to satisfy the relations is initially much larger than the amount of liquid mixed in and, in only a few steps, crystallization far outpaces the observed amount of crystals in the pumices.

(3) The initial slope of the mixing curve (at less than $\sim 0.4\%$ mixed in melt) is greater than that for pure sanidine fractional crystallization. This means that concomitant with initial mixing, sanidine crystallization moves the melt composition in the direction that instead of solving the problem makes it worse. Although not impossible, a mixing and crystallization process is an implausible explanation of almost the entire range of the observed Ba/Rb vs Sr/Rb correlation.

Crystal sinking is an alternative form of mixing and crystallization, because crystals can sink from one part of a magma into another. This process might be termed crystal mixing to emphasize its difference from magma mixing. Sinking of late-erupted quartz and sanidine phenocrysts into less differentiated melt can explain: (1) the reversed zonation of Ba-rich rims on sanidine phenocrysts; (2) CO_2-rich melt inclusions near the rims of quartz phenocrysts; (3) inclusions of early-type magnetite in some late-deposited quartz phenocrysts. Crystal sinking best explains our observations. Implications and tests of crystal sinking are considered further in the next section.

There are two problems with the crystal sinking scenario: (1) we found no early-type (low temperature) magnetite inclusions in late-erupted sanidine phenocrysts; (2) sodic plagioclase cores are rare in late-erupted plagioclase. Phenocrysts of both sanidine and plagioclase are similar in size and density to quartz and would sink at about the same rate as quartz. That we found no early-type magnetite inclusions in sanidine may reflect a sampling accident or reequilibration of magnetite in sanidine via melt channels along cleavage cracks. The precursor magma may have contained very little plagioclase compared with quartz and sanidine. That there are some sodic plagioclase cores in late-erupted plagioclase is consistent with some plagioclase sinking.

Ages of differentiation and crystallization, and the duration of magma storage

We now examine our interpretations for consistency with other studies, some of which have suggested that both differentiation and crystallization of phenocrysts occurred long before eruption. At issue is whether the Bishop phenocrysts and their inclusions relate to the condition of the magma at the time of eruption or at some much earlier time or both. It is important to distinguish between the age of differentiation (how long ago certain compositional variations such as whole-rock Rb/Sr were generated) and the age of phenocryst crystallization. A sufficiently slow rate of crystal growth and/or sinking could result in phenocrysts recording an evolutionary range of conditions during preeruptive magma storage.

A growth rate is implied by our interpretation that reversely zoned sanidine phenocrysts grew as they sank. The implied growth rate is the amount of linear growth divided by the time to sink the indicated distance. The increase in pressure implied by an increase of 552 ppm of CO_2 (in inclusions from core to rim of crystal LV81-18a-132; Fig. 3) is ~ 800 bars or 3·6 km in a melt with a density of 2·2 g/m^3. The Stokes settling rate for a 1 mm quartz crystal in rhyolitic melt is ~ 8 cm/yr [viscosity of Bishop rhyolite melt with 4·3 wt % H_2O at 790°C is 4 $\times 10^6$ poise (Shaw, 1972)], and a crystal such as LV81-18a-132 would require a minimum of ~ 40 ky to sink 3·6 km. The implied maximum average rate of growth is ~ 1 mm per 83 ky [similar to estimates of Christensen & DePaolo (1993) and Davies *et al.* (1994)]. If the phenocryst grew at a constant linear rate, then sinking would take 58 ky and the rate of growth would be 1 mm per 116 ky. Some of the pressurization may have been caused by downward displacement of magma (for example, by superjacent addition of buoyant magma), and this would lessen the duration of sinking. However, movement of phenocrysts relative to melt (sinking) is required to explain the reversed compositional zonation. Our crystal sinking hypothesis yields phenocryst growth rates in the Bishop magma that are consistent with those estimated by other methods.

Our Ba/Sr data can be used to constrain the duration of high-temperature igneous storage between crystallization of the core of the late-erupted sanidine phenocryst 17A-1 (Fig. 9) and its eruption. The core has about 115 ppm Ba and 210 ppm Sr. Using the sanidine–melt partition coefficients discussed above, the melt contained 4·0 ppm Ba and 18·6 ppm Sr. Bishop melt inclusions with ~ 4 ppm Ba have only 1·5–2·2 ppm Sr (Fig. 5). Assuming negligible post-crystallization change in Ba (Ba

diffusivity in rhyolitic melt is about a factor of six smaller than for Sr; Margaritz & Hofmann, 1978), we expect that the sanidine core that formed from a 2 ppm Sr melt would contain 22·6 ppm Sr compared with the observed 210 ppm Sr. The corresponding Fourier number (Dt/a^2, where D is the diffusion coefficient, t is time and a is distance) is 0·13 assuming a fixed Sr concentration of 400 ppm at the perimeter of a core 250 µm in radius, the distance through which diffusion plausibly affected the core. Using the stated uncertainty in the activation energy, the chemical diffusivity of Sr in sanidine (Or_{61} compared with Bishop sanidine Or_{65}) under dry conditions at 780°C is $0·91 \times 10^{-18}$ to $17·7 \times 10^{-18}$ cm^2/s (Cherniak, 1996). The corresponding time for diffusive addition of Sr to the core is $0·14 \times 10^6$ to $2·8 \times 10^6$ years. It is important to note, however, that Giletti (1991) measured a 100 times larger diffusivity of Sr in orthoclase under hydrothermal conditions for self-diffusion (which is more applicable to Sr isotopic exchange than to Sr chemical diffusion). Cherniak & Watson (1992) stated (p. 421): 'A more complete understanding of the effects of water (or other H-bearing species) and pressure on Sr diffusion must await further experimentation'. Thus our estimated time for Sr diffusion in a natural sanidine phenocryst in a hydrous magma is tentative. On the other hand, our compositional data do imply substantial post-formation changes in the Sr concentrations in the cores of some Bishop sanidine phenocrysts. This view contrasts with that of Davies & Halliday (1998), who inferred negligible diffusive exchange of Sr in cores of Bishop as well as Glass Mountain sanidine phenocrysts. During the times required for diffusive exchange, temperature would have to remain at or above ~780°C, or the time would have to be greater, because the diffusivity is sensitive to temperature. If cooling and reheating occurred, as argued by Mahood (1990), the total duration of storage would be longer. Our data thus are tentatively consistent with storage of some late-erupted Bishop magma at ~780°C for 100 ky or more.

Storage of Bishop magma for 100 ky or more has been suggested by Christensen & DePaolo (1993) and Van den Bogaard & Schirnick (1995). Christensen & Halliday (1996) inferred that some Bishop plagioclase and sanidine phenocrysts crystallized ~100 ky before eruption. These interpretations of radiometric analyses allow the possibility that the 'magma' was cool for much of the time; storage times based on diffusivity require the magma to remain hot.

Our melt inclusion data place another limit on the rate of growth of quartz and sanidine in the Bishop magma. Sufficiently rapid growth would require significant concentration gradients in the melt that would be recorded in the compositions of melt inclusions. Lu *et al.* (1995) showed that melt inclusions in early Bishop quartz have compositions consistent with analytically undetectable concentration gradients. There are three lines of evidence. First, if there were significant concentration gradients during growth, then small inclusions would have higher concentrations of incompatible elements than large inclusions. There is no correlation between size and inclusion composition, however. Second, concentrations of elements incompatible in quartz should correlate positively, if the effects of diffusive boundary layers predominated over that of crystallization differentiation. However, incompatible U correlates negatively with compatible trace elements in melt inclusions, consistent with crystallization differentiation and inconsistent with diffusive boundary layer control. Third, aluminum and silicon should be oppositely affected by crystallization of quartz and sanidine; however, the aluminum and silicon concentrations in melt inclusions in both quartz and sanidine are the same within error. Possible post-entrapment diffusive equilibration between melt inclusions and host melt is inconsistent with observed variations in trace element compositions from one inclusion to another in the same pumice clast or crystal. Other than the existence of the phenocrysts, there is no petrographic evidence for a finite rate of their growth.

Lu *et al.* (1995) modeled the formation of inclusions 50 and 400 µm in diameter with 10 µm thick boundary layers and noted that the compositional uniformity and 1·0% error in SiO$_2$ in the melt inclusions, together with a diffusivity of SiO$_2$ of 3×10^{-10} cm^2/s in hydrous rhyolite melt (Baker, 1991), limit the growth rate to $<4 \times 10^{-8}$ cm/s (~1 mm per month) during inclusion entrapment.

Alternatively, we may assume that melt inclusions form during average conditions of crystal growth. In this case, steady-state cocrystallization of quartz and sanidine 'pushes' aluminum away from quartz towards the nearest sanidine surface, yielding a roughly uniform concentration gradient between quartz and sanidine (neglecting nonlinear relations between activity and concentration). The distance between the surfaces of neighboring quartz and sanidine phenocrysts is ~0·5 cm in bubble-free, early Bishop magma (calculated by assuming ~5 vol. % each of 2 mm cubic phenocrysts of quartz and sanidine). The concentration of Al$_2$O$_3$ is likely to change less than that of SiO$_2$ as a result of post-entrapment crystallization or solution of host mineral; therefore, we base this assessment on Al$_2$O$_3$ and assume that the diffusivity of aluminum is about the same as that of silicon. The product of the concentration gradient (<1 wt % change in Al$_2$O$_3$ per 0·5 cm) and the diffusivity equals the linear growth rate times the mass fraction of Al$_2$O$_3$ in sanidine (0·17). Thus the maximum linear growth rate is $\sim 4 \times 10^{-11}$ cm/s (~1 mm per 100 years). Our data on melt inclusions allow the range in Al$_2$O$_3$ as a result of cocrystallization to be less than the 1% analytical error and the actual growth rate may be

correspondingly less. These growth rates, although large, are upper limits and thus are not inconsistent with our estimated growth rate of 1 mm per 100 ky based on crystal sinking time.

Likewise, the above maximum rates of crystallization although greater than are not inconsistent with those based on radiometric dating of Bishop phenocrysts. Christensen & DePaolo (1993) estimated a rate of sanidine growth in the Bishop magma of 10^{-14} cm/s (~ 1 mm per 300 ky). Although Davies *et al.* (1994) and Davies & Halliday (1998) inferred similar rates of feldspar growth in some pre-Bishop Glass Mountain rhyolites, their isotopic data on Bishop phenocrysts and glasses are too complex to allow estimation of a rate of crystallization.

Finally, we should see if rates of crystal growth and sinking are consistent with rates based on the temperature gradient to the surface and the implied heat flux out of the top of the magma body. Temperature rose by $\sim 700°C$ from the surface down to the top of the magma. The depth to the uppermost (and earliest erupted) part of the magma body is constrained by the 1·4 kbar gas-saturation pressures of melt inclusions in some early-erupted quartz phenocrysts [Wallace *et al.* (1999) and earlier works cited there], corresponding to a depth of 5·2 km. The corresponding conductive heat flux to the surface ($T = 25°C$) from 5 km depth ($T = 725°C$) amounts to $\sim 0·4$ W/m^2 (assuming an average thermal conductivity of 3 W/m per K).

Non-convective heat flux through the Bishop magma itself is more difficult to assess because the thermal conductivity of molten silicates is controversial [see discussions by Snyder *et al.* (1995, 1997)] and radiative transport can be significant, particularly in iron-poor melts such as rhyolite. The temperature gradient through the magma can be estimated from the temperature range of $\sim 65°C$ (Hildreth, 1979) and the 5·4 km erupted magma body thickness that is implied by maximum gas-saturation pressures of $\sim 2·6$ kbar for some late-erupted melt inclusions (Wallace *et al.*, 1999). If we assume, for purposes of illustration, that the 'bulk' (radiative plus conductive) thermal conductivity for the iron-poor magma is five times larger than that for the crystalline roof rocks, then the corresponding non-convective heat flux through the magma itself is 0·18 W/m^2. The remaining 0·22 W/m^2 would need to be supplied by latent heat released by the crystallizing magma (Mahood, 1990) or by convective transfer or something else. (The radiogenic heat produced by 5 km of Bishop magma is $\sim 0·02$ W/m^2.) Assuming a latent heat of 60 cal/g for the Bishop magma the downward rate of total crystallization sufficient to supply the heat flux of 0·22 W/m^2 is 9 mm/yr or 0·9 km per 100 ky.

The above rate of crystallization far exceeds all but the estimate of Lu *et al.* (1995) for hypothetical bursts of crystal growth leading to melt inclusion entrapment.

Erupted phenocrysts evidently grew mostly much more slowly, presumably in a less supercooled environment, implying that they did not derive from a rapidly crystallizing roof rind. If the actual heat flux out of the top of the crystalline roof zone were greater because of hydrothermal convective cooling, then the implied rate of crystallization would be correspondingly greater. If the magma convected, or if the effective thermal conductivity in the magma were greater, then the latent heat production and rate of crystallization could be less. Accurate knowledge of the thermal conductivity and radiative properties of rhyolitic magmas would help narrow the options.

To be part of the erupted, slowly crystallized magma the largest crystals in near-roof magma should sink no faster than the crystallization front advances downward; otherwise, they would have sunk away. The largest crystals of quartz in early-erupted Bishop pumices are ~ 3 mm in diameter. Their sink rate would be about six times greater than that for crystal LV81-18a-132 (Fig. 3) or 9 km per 100 ky compared with the above estimate of 0·9 km per 100 ky for the advance of the crystallization front. The factor of 10 discrepancy we regard to be within the present state of knowledge, but it does draw attention to the need for additional work on the transport properties of silicic melts and magmas.

Most of the discussion regarding long-term storage of rhyolitic magma has focused on Glass Mountain (Halliday *et al.*, 1989). The Bishop magma differed from Glass Mountain magma in several respects. (1) The erupted mass exceeds that of all of the Glass Mountain rhyolites by more than a factor of 10. (2) Bishop magmas were comparatively crystal rich (Hildreth, 1977, 1979). (3) The Bishop magma (especially early and mid-erupted magma) was stably stratified (Wallace *et al.*, 1995, 1999). (4) Melt inclusions in Bishop quartz phenocrysts are compositionally different from Glass Mountain rhyolites (Wallace *et al.*, 1999), although there is some overlap in isotopic composition (see, e.g. Christensen & Halliday, 1996). Close association in space and time makes it plausible that there was some genetic relation between Glass Mountain magma and Bishop magma, but transfer of conclusions based on studies of Glass Mountain rhyolites to the Bishop magma should be approached with some skepticism.

With regard to Glass Mountain magmas, Halliday (1990) argued (p. 393) that 'the problems of retaining low-temperature magmas at high levels in the crust are simplified to maintaining a reasonably constant modest heat flux from deeper levels'. Our quantitative assessment given above reveals that, for the Bishop magma, conduction cannot transfer sufficient heat flux from below, although radiation might. Convection could transfer sufficient heat, but convection within the whole body of magma or even thick layers would mix phenocrysts from

various levels and is therefore incompatible with the observed compositional uniformity of phenocrysts in individual pumice clasts or stratigraphic horizons (Hildreth, 1979). To be compatible with the within-clast compositional uniformity of early-erupted phenocrysts, individual clasts must sample less than ~10% of the entire compositional range of Bishop phenocrysts, meaning that for a simple layer-cake magma body convecting layers should be thinner than 500 m. In a crystallizing, gas-saturated magma, the effects of temperature and composition on density are interdependent through the effect of dissolved H_2O on the equilibrium crystallization temperature. Therefore, a standard assessment of the convective regime in terms of compositional (solutal) and thermal Rayleigh numbers (Turner, 1974) is suspect, and the feasibility of thin-layer double-diffusive convection in the Bishop magma is uncertain. The small bodies of magma in the Glass Mountain system, on the other hand, may have been thin enough such that conduction and radiation sufficed to keep them hot.

Derivation of old crystals (xenocrysts) from a rind of largely crystallized magma as suggested by Mahood (1990) for Glass Mountain rhyolites and by Nakada *et al.* (1994) for some Crater Lake magmas is implausible for the Bishop magma, because Bishop phenocrysts of quartz and feldspar are dominantly individual faceted crystals; crystal clots are rare, as also noted by Davies & Halliday (1998, p. 3570: 'all phases studied are euhedral and occur as single unbroken grains'). Clots of crystals could become disaggregated by decompressive expansion of bubbles along grain boundaries, but this would not require that the aggregates derive from the rind of the magma. The observation of Wallace *et al.* (1999) that the range of melt inclusion compositions within individual pumice clasts corresponds to relatively small amounts of crystallization as seen in the actual pumice is more compelling, as a much wider range would be expected for crystals accidentally dislodged from mushy rinds with at least 60% of crystals.

Existing ideas about the development of large bodies of silicic magma invoke a gradual addition of magma into a near-surface reservoir (Smith, 1979). Perhaps successive additions of hot, gassy silicic magma into and above a growing body of resident magma helped maintain the molten lifetime of the Bishop magma. If, as equilibrium would require, crystallization accompanied decompressive additions of gassy magma, then the range of crystallization ages should record the duration of magma reservoir inflation.

Van den Bogaard & Schirnick (1995) reported argon data on melt inclusions in Bishop quartz phenocrysts, which they interpreted to reflect entrapment of the melt inclusions within their quartz hosts at about 1·9 My and 1·2 My before eruption. Alternatively, at the time of entrapment, there might have been a nearly constant concentration of dissolved ^{40}Ar. The K concentration in the eutectoid melt would also be approximately constant, and a uniform apparent $^{40}Ar*/^{39}Ar$ ratio would result. In this alternative scenario, the timing of entrapment within the quartz is constrained to have taken place no earlier than 1·9 Ma, but no later than 0·76 Ma. Argon systematics alone would not be able to narrow the age of entrapment any further.

Apparent ages of differentiation of Bishop magma based on Rb/Sr analyses of melt-inclusion-bearing quartz phenocrysts by Christensen & Halliday (1996) range from 1·4 to 2·5 Ma for early-erupted magma and from 1·0 to 1·2 Ma for some of the late-erupted magma. Rates of crystal sinking, however, reveal that it would be problematic for phenocrysts of quartz to remain suspended in the upper 4 km of the magma body for more than ~100 ky. Christensen & DePaolo (1993) suggested that a finite yield strength prevented phenocrysts from sinking. Although the crystal-rich magma may have had a finite yield strength because of crystal interactions, this does not require that the melt fraction itself had a yield strength capable of preventing crystal sinking. Further tests of crystal sinking are needed.

The Rb/Sr isotopic systematics in Bishop phenocrysts and melts seems complex and the combined effects of crystallization, crystal sinking and diffusive equilibration are difficult to predict. The concentration of Sr in the Bishop melt is sensitive to phenocryst crystallization, and the Rb/Sr ratio in the melt increases by a factor of ~4·4 for 20 wt % of fractional crystallization of a Bishop assemblage. This result assumes perfect fractionation and is based on partition factors and mineral proportions mentioned above [see the section 'Crystal settling (sinking) and/or magma mixing', above]. However, perfect fractional crystallization for the Bishop magma is not certain, and significant equilibration between phenocrysts and liquid would lead to a different result. In fact, the $^{87}Rb/^{86}Sr$ ratio of our melt inclusions in early-erupted quartz phenocrysts ranges from about 200 to 600. Significantly, most of that range is found even among multiple inclusions within individual quartz phenocrysts. Our range is significantly larger than that found by Christensen & Halliday (1996) for a set of four inclusion-bearing quartz phenocrysts. Various stages of differentiation existed in different parts of the erupted magma body at the time of eruption, and this was probably the case long before eruption as well. Melt inclusion entrapment possibly involved liquids with scattered (non-isochron) $^{87}Sr/^{86}Sr$ and $^{87}Rb/^{86}Sr$ consistent with the data of Christensen & Halliday (1996) on Bishop melt inclusions and Knesel & Davidson (1997) on Bishop matrix glasses. Davies & Halliday (1998, p. 3570) concluded: 'true Sr isotope mineral-glass ages cannot be determined on the feldspar population'.

Davies & Halliday (1998) interpreted their isotopic analyses of early Bishop feldspar phenocrysts and associated glasses to signify that many feldspar phenocrysts grew in a different magma, and this too could reflect crystals sinking into layers of magma that had differentiated at various times. However, we do not know if the isotopically distinct crystals occurred together in the same pumice clast. Evidently, coeruption of separate parts of the magma is possible.

By way of summary, we return to Hildreth's (1977, 1979) rejection of crystal settling and convection. He documented that, although there is a significant range in phenocryst compositions throughout the entire Bishop Tuff, within stratigraphically similar samples having similar magnetite–ilmenite equilibration temperatures, phenocryst compositions are practically constant both within individual grains and from grain to grain and pumice clast to pumice clast. Thus there could be no mixing of crystals from one thermal environment to another. As either crystal settling or convection would mix crystals, neither of these could have occurred.

We have made new observations: the sanidines are reversely zoned, early-type magnetites occur enclosed in some late-erupted quartz phenocrysts, and some late-erupted quartz phenocrysts have melt inclusions with high CO_2 and high gas-saturation pressures nearest the crystal rims. Our interpretation is thus different: some quartz and sanidine crystals sank. If these sank no more than ~ 4 km, then crystals of zircon, which are mostly less than 1/20th the size of the millimeter-sized quartz and sanidine, and have only about five times the density contrast, would sink only 50 m. Magnetite phenocrysts would sink only ~ 100 m. This is not far enough to yield detectable mixing of phenocrysts. Although Hildreth's (1977, 1979) argument against convective mixing remains valid, limited crystal sinking is the best explanation of the reversely zoned phenocrysts and is consistent with undetectable mixing of small-sized phenocrysts of magnetite and zircon.

Returning to the issue regarding the record preserved in phenocrysts and their inclusions, we think that our observations, considered in the context of the isotopic chronometric studies of the Bishop Tuff mentioned above, record a long history of magmatic evolution. This history spans at least ~ 100 ky, sufficient time for crystal sinking, crystal growth, crystal zoning and diffusive equilibration. We think, but cannot prove, that these processes continued in the Bishop magma until eruptive quenching.

CONCLUSIONS

The early-erupted Bishop Tuff is a high-silica rhyolite whose magma contained relatively uniform and highly differentiated crystals and melt. It closely approximated a eutectic system. It is a residual magma derived from some parental magma and not itself a primary or parental partial melt of common crustal rocks. These conclusions affirm previous work and interpretations of Hildreth (1977, 1979) and others.

On the basis of new partition coefficients for Ba and Sr derived from our melt inclusion analyses (Lu *et al.*, 1992*b*), the amount of crystallization differentiation required to explain the very low Ba and Sr in the early-erupted Bishop magma is reasonable. The volume of crystalline differentiate can be less than half that of the erupted Bishop magma.

The evolution of the late-erupted magma is constrained by: (1) mostly relatively late eruption from a system of vents north of and separate from the southern, early-erupting vents (Wilson & Hildreth, 1997); (2) reversed compositional zoning of sanidine phenocrysts and melt inclusions in quartz phenocrysts, consistent with crystals growing from successively less differentiated melts; (3) highly variable CO_2/H_2O in melt inclusions, suggestive of gas-saturated growth of phenocrysts and entrapment of melt inclusions; (4) CO_2-rich melt inclusions with relatively high gas-saturation pressures preferentially located near the rims of quartz phenocrysts, consistent with progressive increase in pressure of crystallization plausibly by crystal settling; (5) positive correlation between CO_2 and Ba in melt inclusions, compatible with (2) and (4) above; (6) a population of relatively highly-differentiated (early, low-T type) magnetite inclusions in late-erupted phenocrysts of quartz, signifying derivation of some late-erupted phenocrysts from a more differentiated magma similar to that of the early-erupted magma; (7) a linear relation between log(Ba/Rb) and log(Sr/Rb) in melt inclusions that is difficult to reconcile with magma mixing even if combined with fractional crystallization. We cannot exclude magma mixing, particularly for some of the least differentiated, most Ba-rich melts. However, the most plausible interpretation is one whereby initial phenocrysts crystallized as gas-saturated batches of magma ascended into magma reservoirs about 4–10 km below the surface. Concomitantly with crystallization, some crystals sank into less differentiated magmas (Fig. 13). The magma that erupted to form the early-erupted highly differentiated magma had evolved further as early phenocrysts sank out of it. As a result, there are some moderately differentiated melt inclusions in late-erupted quartz, which probably are samples of melt that existed earlier, closer to the time of initial emplacement. The initial magma in the upper parts of the magma body, although compositionally close to the early-erupted magma, was less differentiated. Before eruption some crystals sank out of it, and it thereby evolved to the even more differentiated melt and magma that erupted early.
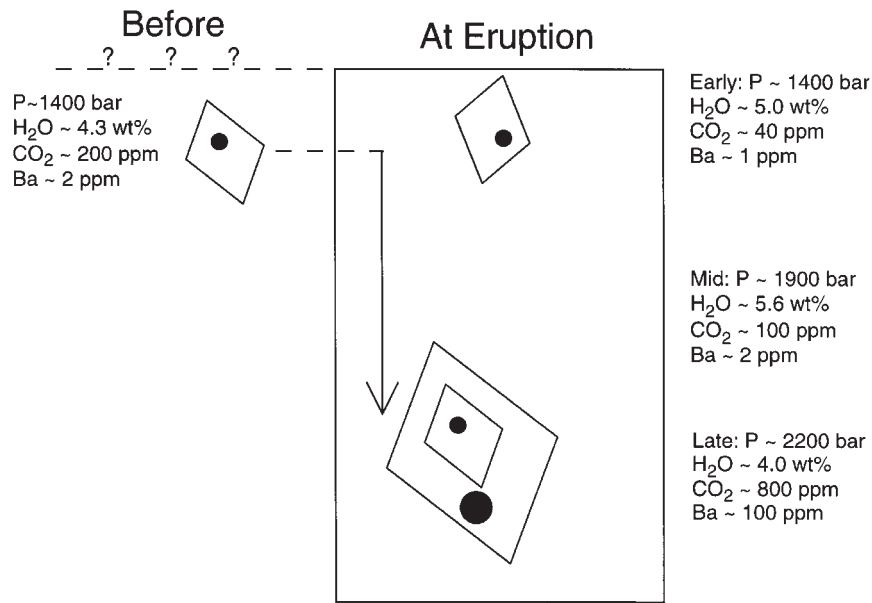
Before

_ _?_ _?_ _?_ _

P~1400 bar
H_2O ~ 4.3 wt%
CO_2 ~ 200 ppm
Ba ~ 2 ppm

At Eruption

Early: P ~ 1400 bar
H_2O ~ 5.0 wt%
CO_2 ~ 40 ppm
Ba ~ 1 ppm

Mid: P ~ 1900 bar
H_2O ~ 5.6 wt%
CO_2 ~ 100 ppm
Ba ~ 2 ppm

Late: P ~ 2200 bar
H_2O ~ 4.0 wt%
CO_2 ~ 800 ppm
Ba ~ 100 ppm

Fig. 13. Sketch showing the inferred scheme of crystallization and differentiation of the magma body that erupted to form the Bishop Tuff. Before eruption melt inclusions (black circle) were trapped in growing phenocrysts of quartz (diamond-shaped box), some like inclusion 3 in crystal 132 (see Fig. 3) at a gas-saturation pressure of ∼1400 bars. This initial, precursor melt was only moderately differentiated and contained ∼2 ppm Ba, judging from the Ba vs CO_2 correlation (Fig. 6). When eruption began some crystals (such as crystal 132, Fig. 3) had sunk into even less differentiated melt and some of this melt (large black circle) became entrapped in the outer parts of the quartz phenocryst at ∼2200 bars. In the upper part, a body of highly differentiated melt had evolved by loss of crystals, and new crystals trapped some of this highly differentiated melt (commonly with 1 ppm or less of Ba) as they grew. Additional magma evolved at mid levels (∼1900 bars) and contained crystals (not shown) most of which trapped moderately differentiated melt and did not sink far before eruption.

Some of the crystals that sank out of the initial magma were erupted in late-erupted magma.

Larger significance

It is important to understand how large bodies of silicic magma work, because their evolution is an important aspect of planetary differentiation. What we conclude from our work is that the strictly compositional aspects of magmatic evolution in the Bishop system are well in accord with crystallization differentiation. An upper portion of the magma body was highly differentiated. This might arise in several ways: (1) highly differentiated residual melt might migrate from source veins and come to occupy the shallowest levels of the magma body simply because the most differentiated melts are the most buoyant; (2) such melt might evolve by growth of crystals attached to the walls and roof of a largely molten body; (3) such melt might develop as a residuum left behind as crystals sank out of it. Our work points to option (3), as this is the only option that can both readily account for reversely zoned phenocrysts and at the same time produce highly differentiated magma. Option (1) may have played a significant role initially as the magma body grew. Reversely zoned phenocrysts are conspicuous in other silicic ash-flow tuffs and are not unique to the Bishop

system (indeed the Bishop phenocrysts are exceptionally uniform). Option (3) is the one most sensitive to H_2O and its effect on diminishing the viscosity of the melt (so that the phenocrysts can sink at a rate that is competitive with the downward rate of advance of the crystallization front). If crystal sinking and buoyant rise are the main mechanisms for the formation of highly silicic magmas, then planetary evolution of highly silicic (granitic) crusts will be favored on larger (highly gravitating), wet planets. This seems to be consistent with what planetary investigations have revealed about the Moon, Mars and Venus as compared with Earth.

REFERENCES

Bacon, C. R., Newman, S. & Stolper, E. (1992). Water, CO_2, and F in melt inclusions in phenocrysts from three Holocene explosive eruptions, Crater Lake, Oregon. *American Mineralogist* **77**, 1021–1030.

Baker, D. R. (1991). Interdiffusion of hydrous dacitic and rhyolitic melts and the efficacy of rhyolite contamination of dacitic enclaves. *Contributions to Mineralogy and Petrology* **106**, 462–473.

Best, M. G. & Christiansen, E. H. (1997). Origin of broken phenocrysts in ash-flow tuffs. *Geological Society of America Bulletin* **109**, 63–73.

Bindeman, I. N., Davis, A. M. & Drake, M. J. (1998). Ion microprobe study of plagioclase–basalt partition experiments at natural concentration levels of trace elements. *Geochimica et Cosmochimica Acta* **62**, 1175–1193.

Blake, S. & Ivey, G. N. (1986). Magma-mixing and the dynamics of withdrawal from stratified reservoirs. *Journal of Volcanology and Geothermal Research* **27**, 154–178.

Blank, J. G. (1993). An experimental investigation of the behavior of carbon dioxide in rhyolitic melt. Ph.D. Dissertation, California Institute of Technology, Pasadena, 227 pp.

Blank, J. G., Stolper, E. M., Sheng, J. & Epstein, S. (1989). The solubility of CO_2 in rhyolitic melt at pressures to 1500 bars. *Geological Society of America, Abstracts with Programs* **21**, A157.

Blank, J. G., Stolper, E. M. & Carroll, M. R. (1993). Solubilities of carbon dioxide and water in rhyolitic melt at 850°C and 750 bars. *Earth and Planetary Science Letters* **119**, 27–36.

Blundy, J. D. & Wood, B. J. (1991). Crystal-chemical controls on the partitioning of Sr and Ba between plagioclase feldspar, silicate melts, and hydrothermal solutions. *Geochimica et Cosmochimica Acta* **55**, 193–209.

Burnham, C. W. & Jahns, R. H. (1962). A method for determining the solubility of water in silicate melts. *American Journal of Science* **260**, 721–745.

Cameron, K. L. (1984). Bishop Tuff revisited: new rare earth element data consistent with crystal fractionation. *Science* **224**, 1338–1340.

Cherniak, D. J. (1996). Strontium diffusion in sanidine and albite, and general comments on strontium diffusion in alkali feldspars. *Geochimica et Cosmochimica Acta* **60**, 5037–5043.

Cherniak, D. J. & Watson, E. B. (1992). A study of strontium diffusion in K-feldspar, Na–K feldspar and anorthite using Rutherford backscattering spectroscopy. *Earth and Planetary Science Letters* **113**, 411–425.

Christensen, J. N. & DePaolo, D. J. (1993). Timescale of large volume silicic magma systems: Sr isotopic systematics of phenocrysts and glass from the Bishop Tuff, Long Valley, California. *Contributions to Mineralogy and Petrology* **113**, 100–114.

Christensen, J. N. & Halliday, A. N. (1996). Rb–Sr ages and Nd isotopic compositions of melt inclusions from the Bishop Tuff and the generation of silicic magma. *Earth and Planetary Science Letters* **144**, 547–561.

Davis, A. M., MacPherson, G. J., Clayton, R. N., Mayeda, T. K., Sylvester, P. J., Grossman, L., Hinton, R.W. & Laughlin, J. R. (1991). Melt solidification and late-stage evaporation in the evolution of a FUN inclusion from the Vigarano C3V chondrite. *Geochimica et Cosmochimica Acta* **55**, 621–637.

Davies, G. R. & Halliday, A. N. (1998). Development of the Long Valley rhyolitic magma system: strontium and neodymium isotope evidence from glasses and individual phenocrysts. *Geochimica et Cosmochimica Acta* **62**, 3561–3574.

Davies, G. R., Halliday, A. N., Mahood, G. A. & Hall, C. M. (1994). Isotopic constraints on the production rates, crystallization histories and residence times of pre-caldera silicic magmas, Long Valley, California. *Earth and Planetary Science Letters* **125**, 17–37.

Dunbar, N. W. & Hervig, R. L. (1992). Petrogenesis and volatile stratigraphy of the Bishop Tuff: evidence from melt inclusion analysis. *Journal of Geophysical Research* **97**, 15129–15150.

Gilbert, C. M. (1938). Welded Tuff in eastern California. *Geological Society of America Bulletin* **49**, 1829–1862.

Giletti, B. J. (1991). Rb and Sr diffusion in feldspars, with implications for cooling histories of rocks. *Geochimica et Cosmochimica Acta* **55**, 1331–1343.

Halliday, A. N., Fallick, A. E., Hutchinson, J. & Hildreth, W. (1984). A Nd, Sr and O isotopic investigation into the causes of chemical and isotopic zonation in the Bishop Tuff, California. *Earth and Planetary Science Letters* **68**, 379–391.

Halliday, A. N. (1990). Reply to comment of R. S. J. Sparks, H. E. Huppert, & C. J. N. Wilson on 'Evidence for long residence times of rhyolitic magma in the Long Valley magmatic system: the isotopic record in the precaldera lavas of Glass Mountain'. *Earth and Planetary Science Letters* **99**, 390–394.

Halliday, A. N., Mahood, G. A., Holden, P., Metz, J. M., Dempster, T. J. & Davidson, J. P. (1989). Evidence for long residence times of rhyolitic magma in the Long Valley magmatic system: the isotopic record in the precaldera lavas of Glass Mountain. *Earth and Planetary Science Letters* **94**, 274–290.

Hervig, R. L. & Dunbar, N. W. (1992). Causes of chemical zoning in the Bishop (California) and Bandelier (New Mexico) magma chambers. *Earth and Planetary Science Letters* **111**, 97–108.

Hildreth, E. W. (1977). The magma chamber of the Bishop Tuff: gradients in temperature, pressure and composition. Ph.D. Dissertation, University of California, Berkeley, 328 pp.

Hildreth, E. W. (1979). The Bishop Tuff: evidence for the origin of the compositional zonation in silicic magma chambers. *Geological Society of America, Special Paper* **180**, 43–76.

Hildreth, E. W. (1981). Gradients in silicic magma chambers: implication for lithospheric magmatism. *Journal of Geophysical Research* **86**, 10153–10192.

Hildreth, W. (1985). The Bishop Tuff: trace contents of dark pumice. *Geological Society of America, Abstracts with Programs* **17**, 361.

Hildreth, W. & Mahood, G. A. (1986). Ring-fracture eruption of the Bishop Tuff. *Geological Society of America Bulletin* **97**, 396–403.

Hinton, R. W., Davis, A. M., Scatena-Wachel, D. E., Grossman, L. & Draus, R. J. (1988). A chemical and isotopic study of hibonite-rich refractory inclusions in primitive meteorites. *Geochimica et Cosmochimica Acta* **52**, 2573–2598.

Knesel, K. M. & Davidson, J. P. (1997). The origin and evolution of large-volume silicic magma systems: Long Valley Caldera. *International Geology Review* **39**, 1033–1052.

Lu, F. (1991). The Bishop Tuff: origins of the high-silica rhyolite and its thermal and chemical zonations. Ph.D. Dissertation, University of Chicago, 313 pp.

Lu, F. & Anderson, A. T. (1991). Mixing origins of volatile and thermal gradients in the Bishop magma. *EOS Transactions, American Geophysical Union* **72**, 312.

Lu, F., Anderson, A. T. & Davis, A. M. (1992a). Melt inclusions and crystal–liquid separation in rhyolitic magma of the Bishop Tuff. *Contributions to Mineralogy and Petrology* **110**, 113–120.

Lu, F., Anderson, A. T. & Davis, A. M. (1992b). New and larger sanidine/melt partition coefficients for Ba and Sr as determined by ion microprobe analyses of melt inclusions and their sanidine host crystals. *Geological Society of America, Abstracts with Programs* **24**, A44.

Lu, F., Anderson, A. T. & Davis, A. M. (1995). Diffusional gradients at the crystal/melt interface and their effect on the composition of melt inclusions. *Journal of Geology* **103**, 591–597.

MacPherson, G. J. & Davis, A. M. (1994). Refractory inclusions in the prototypical CM chondrite, Mighei. *Geochimica et Cosmochimica Acta* **58**, 5599–5625.

Mahood, G. A. (1990). Second reply to comment of R. S. J. Sparks, H. E. Huppert and C. J. N. Wilson on 'Evidence for long residence times of rhyolitic magma in the Long Valley magmatic system: the isotopic record in the precaldera lavas of Glass Mountain'. *Earth and Planetary Science Letters* **99**, 395–399.

Margaritz, M. & Hofmann, A. W. (1978). Diffusion of Sr, Ba, and Na in obsidian. *Geochimica et Cosmochimica Acta* **42**, 595–605.

Michael, P. J. (1983). Chemical differentiation of the Bishop Tuff and other high-silica magmas through crystallization processes. *Geology* **11**, 31–34.

Nakada, S., Bacon, C. R. & Gartner, A. E. (1994). Origin of phenocrysts and compositional diversity in pre-Mazama rhyodacite lavas, Crater Lake, Oregon. *Journal of Petrology* **35**, 127–162.

Newman, S., Epstein, S. & Stolper, E. (1986). Measurement of water in rhyolitic glasses: calibration of an infrared spectroscopic technique. *American Mineralogist* **71**, 1527–1541.

Newman, S., Epstein, S. & Stolper, E. (1988). Water, carbon dioxide and hydrogen isotopes in glasses from the ca. 1340 AD eruption of the Mono Craters, California: constraints on degassing phenomena and initial volatile content. *Journal of Volcanology and Geothermal Research* **35**, 75–96.

Puchelt, H. (1972). Barium. In: Wedepohl, K. H. (ed.) *Handbook of Geochemistry*. Berlin: Springer-Verlag, pp. 56-B–56-O.

Qin, Z. (1994). Melting and diffusive equilibration in igneous processes. Ph.D. Thesis, University of Chicago, 138 pp.

Schuraytz, B. C., Vogel, T. A. & Younker, L. W. (1989). Evidence for dynamic withdrawal from a layered magma body: the Topopah Spring Tuff, Southwestern Nevada. *Journal of Geophysical Research* **94**, 5925–5942.

Shaw, H. R. (1972). Viscosities of magmatic silicate liquids: an empirical method of prediction. *American Journal of Science* **272**, 870–893.

Sheridan, M. F. (1965). The mineralogy and petrology of the Bishop Tuff. Ph.D. Thesis, Stanford University, Palo Alto, CA, 165 pp.

Silver, L. A., Ihinger, P. D. & Stolper, E. (1990). The influence of bulk composition on the speciation of water in silicate glasses. *Contributions to Mineralogy and Petrology* **104**, 142–162.

Simon, S. B., Grossman, L. & Davis, A. M. (1991). Fassaite composition trends during crystallization of Allende type B refractory inclusion melts. *Geochimica et Cosmochimica Acta* **55**, 2635–2655.

Skirius, C. M. (1990). Pre-eruptive H_2O and CO_2 content of the plinian and ash-flow Bishop Tuff magma. Ph.D. Thesis, University of Chicago, 237 pp.

Skirius, C. M., Peterson, J. W. & Anderson, A. T., Jr (1990). Homogenizing rhyolitic glass inclusions from the Bishop Tuff. *American Mineralogist* **75**, 1381–1398.

Smith, R. L. (1979). Ash-flow magmatism. *Geological Society of America, Special Paper* **180**, 5–27.

Smith, R. L. & Bailey, R. A. (1966). The Bandelier Tuff: a study of ash-flow eruption cycles from zoned magma chambers. *Bulletin Volcanologique* **29**, 83–104.

Snyder, D., Gier, E. & Carmichael, I. (1995). Reply. *Journal of Geophysical Research* **100**, 22403–22405.

Snyder, D., Gier, E. & Carmichael, I. (1997). Reply. *Journal of Geophysical Research* **102**, 15077–15080.

Spera, F. J., Yuen, D. A., Greer, J. C. & Sewell, G. (1986). Dynamics of magma withdrawal from stratified magma chambers. *Geology* **14**, 723–726.

Tait, S. (1992). Selective preservation of melt inclusions in igneous phenocrysts. *American Mineralogist* **77**, 146–155.

Turner, J. S. (1974). Double-diffusive phenomena. *Annual Reviews of Fluid Mechanics* **6**, 37–56.

Van den Bogaard, P. & Schirnick, C. (1995). $^{40}Ar/^{39}Ar$ laser probe ages of Bishop Tuff quartz phenocrysts substantiate long-lived silicic magma chamber at Long Valley, United States. *Geology* **23**, 759–762.

Wallace, P. J., Anderson, A. T. & Davis, A. M. (1995). Quantification of pre-eruptive exsolved gas contents in silicic magmas. *Nature* **377**, 612–616.

Wallace, P. J., Anderson, A. T. & Davis, A. M. (1999). Gradients in H_2O, CO_2, and exsolved gas in a large-volume silicic magma system: interpreting the record preserved in melt inclusions from the Bishop Tuff. *Journal of Geophysical Research* **104**, 20097–20122.

Williamson, J. H. (1968). Least squares fitting of a straight line. *Canadian Journal of Physics* **46**, 1845–1847.

Wilson, C. J. N. & Hildreth, W. (1997). The Bishop Tuff: new insights from eruptive stratigraphy. *Journal of Geology* **105**, 407–439.

Zhang, Y., Belcher, R., Ihinger, P. D., Wang, L., Xu, Z. & Newman, S. (1997). New calibration of infrared measurement of dissolved water in rhyolitic glasses. *Geochimica et Cosmochimica Acta* **61**, 3089–3100.

APPENDIX: LOCATIONS AND STRATIGRAPHIC RELATIONS OF SAMPLES

Sample location 1 [identical with B 104 of Hildreth (1977) and locality 15 of Wilson & Hildreth (1997)], from which most of our plinian and Chidago samples are derived, is in the main east-trending axis of maximum plinian depositional thickness (~ 34 km east of the vent near the southern Long Valley caldera rim) and exposes

~4 m of plinian pumice fall overlain by and intercalated with ~10 m of Chidago ash-flow deposits. On the basis of Skirius' (1990 and unpublished notes) descriptions and measurements of distance above the base we relate the samples to the Wilson & Hildreth (1997) stratigraphy as follows: BT87-2 is equivalent to F5; BT87-3 is equivalent to F6; BT87-5 to -9 are equivalent to F7; BT87-10 to -16 are equivalent to Ig1Eb.

Sample location 2 (a roadcut on the north side of US 395 ~3 km east of Toms Place, Wilson & Hildreth location 19) is 14 km SE of the vent on the southern caldera rim and exposes ~3 m of plinian deposit on Sherwin Till with another 8 m of exposed roadcut in overlying ash-flow material. Our plinian samples from this locality (BT87-20 to -23) are from F5 and/or F6 of Wilson & Hildreth (1997). Our ash-flow samples (BT87-24 and -25) are mostly or entirely from Ig1Eb. Possibly, but unlikely, a part of BT87-25 is from Ig1Ea.

Sample location 3 [below the Pleasant Valley Dam ~11 km NW of Bishop, approximately locality 24 of Wilson & Hildreth (1997)] is ~34 km SE of the southern vent. The stratigraphic position of our samples from this location is uncertain. However, rhyolite lithic fragments occur both in ash-flow material and in the extreme top of the underlying plinian material (E. W. Hildreth, personal communication, 1993; Wilson & Hildreth, 1997). Our location 3 samples (BT87-131 to -133) are of near-basal ash-flow material and are thus from Ig2Ea.

Sample location 4 [NE1/4 NW1/4 sec. 36 T1S R29E (UTM Grid coord: 4187·1N and 347·7 E), Glass Mountain (1:62 500) quadrangle, E. W. Hildreth, personal communication (1993); 5 km SE of locality 301 of Wilson & Hildreth (1997)] yielded a variety of pumice blocks from hillslope debris derived from the Adobe ash-flow lobe ~8 km north of the caldera rim. The Adobe ash-flow lobe contains abundant, large, crystal-rich, pyroxene-phyric pumice clasts that are similar to some pumice clasts found in the stratigraphically youngest parts of the ash flows south of the caldera (Wilson & Hildreth, 1997). The Adobe ash-flow lobe also contains abundant rhyolitic rock fragments, as do the youngest ash flows preserved south of the caldera. Samples BT87-103 to -123 are from this area and are Ig2Nb.

Sample location 5 [Aeolian Buttes ~1 km east of US 395 and 3 km south of the intersection with California highway 120, ~1·6 km east of and at about the same elevation as locality 104 of Wilson & Hildreth (1997)] contains numerous pinnacles, of 5–8 m height, of slightly welded Mono ash-flow lobe material together with knobs of granite and bouldery Sherwin Till. Although we did not find ash flow in direct contact with either the till or the granite, it is evident from the distribution of outcrops that our samples, which are from near the base of the ash-flow pinnacles, are within ~5 m or less of the underlying pre-Bishop till and granite. Densely welded Mono ash flow occurs nearby at lower elevations and it is evident that the weakly welded ash-flow pinnacles owe their condition to having been deposited on a local, pre-Bishop hill. There is no sign of plinian fall material intervening between the ash flow and the pre-Bishop till and granite. Like the Adobe ash-flow lobe, the Mono ash-flow lobe is rich in large, crystal-rich pumice clasts. Our samples (LV81-17 and -18) from this location are part of Ig2NWb, which is synchronous with Ig2N.

Sample location 6 [roadcut on the NE side of US 395 ~1 km NW of the Crestview highway maintenance station and 3 km NW of the caldera rim, same as locality 208 of Wilson & Hildreth (1997)] exposes nonwelded Mono ash-flow material lying on a weakly developed brownish soil overlying Sherwin Till. The pumice clasts from this locality (our samples 327), although predominantly crystal rich, are smaller than those at location 5, but increase in size upwards. There is a conspicuous horizon rich in large fragments of dark basaltic and intermediate volcanic as well as granitoid rocks ~6 m above the base of the ash flow. This proximal, nonwelded basal part of the Mono ash-flow lobe is basal Ig2NWa and slightly older than our samples from location 5.

Sample location 7 [Top of Owens River Gorge, ~18 km SE of the caldera rim, in SW corner of sec. 22, T 5 S, R 31 E (UTM Grid coord: 4150·6 N and 361·8 E), Mt Tom (1:62 500) quadrangle, located ~10 km NW of location 24 of Wilson & Hildreth (1997)]. Samples LV81-2 to -7 were collected by Druitt & Nagle in 1981 from exposures of non-welded ash-flow material between fumarolic mounds. Ash flows exposed on the surface of the Tableland in this region typically contain pyroxene-phyric pumice and rhyolitic rock fragments. Our samples probably are of unit Ig2E of Wilson & Hildreth (1997). Together with samples from location 3, our samples from location 7 are the youngest material that we studied, which is from south of the caldera rim.